









Cumulative impacts across Australia's Great Barrier Reef: a mechanistic evaluation

YVES-MARIE BOZEC ^{1,5} KARLO HOCK ¹ ROBERT A. B. MASON ¹ MARK E. BAIRD ²
 CAROLINA CASTRO-SANGUINO ¹ SCOTT A. CONDIE ² MARJI PUOTINEN ³ ANGUS THOMPSON,⁴ AND
 PETER J. MUMBY ¹

¹Marine Spatial Ecology Lab, School of Biological Sciences & ARC Centre of Excellence for Coral Reef Studies, University of Queensland, St Lucia, Queensland 4072 Australia

²CSIRO Oceans and Atmosphere, Hobart, Tasmania 7001 Australia

³Australian Institute of Marine Science & Indian Ocean Marine Research Centre, Crawley, Western Australia 6009 Australia

⁴Australian Institute of Marine Science, Townsville, Queensland 4810 Australia

Citation: Bozec, Y.-M., K. Hock, R. A. B. Mason, M. E. Baird, C. Castro-Sanguino, S. A. Condie, M. Puotinen, A. Thompson, and P. J. Mumby. 2021. Cumulative impacts across Australia's Great Barrier Reef: a mechanistic evaluation. *Ecological Monographs* 00(00):e01494. 10.1002/ecm.1494

Abstract. Cumulative impacts assessments on marine ecosystems have been hindered by the difficulty of collecting environmental data and identifying drivers of community dynamics beyond local scales. On coral reefs, an additional challenge is to disentangle the relative influence of multiple drivers that operate at different stages of coral ontogeny. We integrated coral life history, population dynamics, and spatially explicit environmental drivers to assess the relative and cumulative impacts of multiple stressors across 2,300 km of the world's largest coral reef ecosystem, Australia's Great Barrier Reef (GBR). Using literature data, we characterized relationships between coral life history processes (reproduction, larval dispersal, recruitment, growth, and mortality) and environmental variables. We then simulated coral demographics and stressor impacts at the organism (coral colony) level on >3,800 individual reefs linked by larval connectivity and exposed to temporally and spatially realistic regimes of acute (crown-of-thorns starfish outbreaks, cyclones, and mass coral bleaching) and chronic (water-quality) stressors. Model simulations produced a credible reconstruction of recent (2008–2020) coral trajectories consistent with monitoring observations, while estimating the impacts of each stressor at reef and regional scales. Overall, simulated coral populations declined by one-third across the GBR, from an average of ~29% to ~19% hard coral cover. By 2020, <20% of the GBR had coral cover higher than 30%, a status of reef health corroborated by scarce and sparsely distributed monitoring data. Reef-wide annual rates of coral mortality were driven by bleaching (48%) ahead of cyclones (41%) and starfish predation (11%). Beyond the reconstructed status and trends, the model enabled the emergence of complex interactions that compound the effects of multiple stressors while promoting a mechanistic understanding of coral cover dynamics. Drivers of coral cover growth were identified; notably, water quality (suspended sediments) was estimated to delay recovery for at least 25% of inshore reefs. Standardized rates of coral loss and recovery allowed the integration of all cumulative impacts to determine the equilibrium cover for each reef. This metric, combined with maps of impacts, recovery potential, water-quality thresholds, and reef state metrics, facilitates strategic spatial planning and resilience-based management across the GBR.

Key words: coral populations; crown-of-thorns starfish; cyclones; disturbances; heat stress; individual-based model; life history; resilience; spatial simulations; strategic management; water quality.

INTRODUCTION

The increasing threats faced by marine ecosystems compels us to better understand the cumulative impacts of multiple pressures on species and habitats. Yet, progress toward assessment of multiple stressors has been hindered by the difficulty of characterizing biological

responses across ecological scales (Crain et al. 2008, Hodgson and Halpern 2019). Responses to a particular stressor can be complex (e.g., indirect, nonlinear), variable in space and time, and compounded with other stressors or ecological processes (Paine et al. 1998, Darling and Côté 2008). Moreover, one stressor can affect specific life stages or demographic processes that make interactions with other stressors difficult to detect. Integrated approaches to cumulative impact assessment are required to better predict the ecosystem-level effects of multiple stressors and provide enhanced guidance for

Manuscript received 20 November 2020; revised 7 June 2021; accepted 23 July 2021. final version received 20 October 2021.
 Corresponding Editor: Marissa L. Baskett.

⁵E-mail: y.bozec@uq.edu.au

the strategic planning and spatial prioritization of management interventions (Halpern and Fujita 2013, Hodgson and Halpern 2019).

The impacts of multiple stressors can be particularly difficult to predict in biogenic habitats (e.g., coral reefs, kelp forests) where acute and chronic pressures simultaneously affect the reproduction, growth, and mortality of habitat forming species (Harborne et al. 2017, Filbee-Dexter and Wernberg 2018). This is especially challenging on coral reefs, which are deteriorating worldwide due to the compounded effects of natural disturbances with accelerating anthropogenic pressures (Hoegh-Guldberg et al. 2007, Hughes et al. 2017). Whereas extensive coral loss can be easily attributed to acute stressors such as tropical storms, coral bleaching, and outbreaks of coral predators (Hughes and Connell 1999, De'ath et al. 2012), identifying the causes of hindered coral recovery is more difficult (Graham et al. 2011, 2015, Osborne et al. 2017, Ortiz et al. 2018). Slow regeneration of coral populations can result from the dysfunction of a range of early life processes, including reproduction, larval dispersal, settlement, and post-settlement growth and mortality (Hughes and Connell 1999, Hughes et al. 2011). The underlying causes can be multiple, such as macroalgal overgrowth, excess sediment and nutrient from land run-off, and light reduction in turbid waters (Hughes et al. 2003, Fabricius 2005, Mumby and Steneck 2008, Jones et al. 2015, Evans et al. 2020), and attribution can be difficult without surveying the relevant life-history stages. Moreover, response to stressors vary among coral species (Loya et al. 2001, Darling et al. 2013) and can lead to complex interactions whose outcomes are difficult to predict (Ban et al. 2014, Bozec and Mumby 2015). As the focus of modern reef management is on promoting local coral recovery in the face of less manageable drivers (e.g., anthropogenic climate warming), cumulative impacts assessments on coral reefs must integrate all stressors across the coral life cycle.

Australia's Great Barrier Reef (GBR) exemplifies the challenge of evaluating cumulative pressures on coral reefs, despite being widely considered one of the best studied, monitored, and managed reef systems in the world (GBRMPA 2019, although see Brodie and Waterhouse 2012). The GBR Marine Park stretches over 2,300 km across an area of >344,000 km², which means that only a limited fraction of coral reefs can be monitored. Over the past three decades, average coral condition across the GBR has declined in response to the combined impacts of tropical cyclones (TC), outbreaks of the coral-eating crown-of-thorns starfish (*Acanthaster* spp.; CoTS), temperature-induced bleaching, and poor water quality (Osborne et al. 2011, De'ath et al. 2012, Hughes et al. 2017, Schaffelke et al. 2017). Much of the research on cumulative impacts on the GBR has used time series of coral cover to evaluate the rate and drivers of coral loss (Thompson and Dolman 2010, Osborne et al. 2011, Sweatman et al. 2011, De'ath et al. 2012, Cheal et al. 2017). Until recently, coral loss was mostly

related to tropical storms and CoTS outbreaks (De'ath et al. 2012), with occasional yet significant impacts of coral bleaching (Berkelmans et al. 2004, Hughes et al. 2017). The two consecutive bleaching events in 2016 and 2017 that caused extensive coral mortality on the northern two-thirds of the GBR (Hughes et al. 2017, 2018, GBRMPA 2019), extend the relative impact and sphere of influence across the GBR. Anthropogenic climate warming and the reducing time interval between severe bleaching events are now considered a major threat for the GBR, hindering its ability to recover from other disturbances and maintain key reef functions (Schaffelke et al. 2017, GBRMPA 2019).

Compared to drivers of coral loss, pressures on coral recovery across the GBR are less well established. While run-off of fine sediments, nutrients, and pesticides combine to affect water quality on inshore reefs (Brodie and Waterhouse 2012, Schaffelke et al. 2017, Waterhouse et al. 2017), their demographic impacts on corals remain hard to quantify, likely involving interrelated factors such as a reduction in juvenile densities, increased susceptibility to disease, macroalgal growth, and enhanced survival of CoTS larvae (Fabricius and De'ath 2004, Brodie et al. 2005, Fabricius et al. 2010, Thompson et al. 2014). Analyses of monitoring data have related reductions in the rate of coral cover growth with exposure to river plumes (Ortiz et al. 2018, MacNeil et al. 2019) but the underlying mechanisms remain unclear. A number of physiological responses to water-quality parameters have been established experimentally (Fabricius 2005) but quantifying the ecological effects of these responses (e.g., on coral cover) is difficult.

To address the challenges of capturing the impacts of multiple stressors across the GBR, several studies have taken a modeling approach whereby coral loss and recovery are integrated into statistical and/or simulation models of coral cover change (reviewed in Bozec and Mumby 2020, see also Vercelloni et al. 2017, Condie et al. 2018, Lam et al. 2018, Mellin et al. 2019). In these studies, coral population dynamics have been modeled as temporal changes in coral cover, most likely because this is the primary variable that is surveyed in monitoring programs. Although coral cover is a common metric of reef health, it does not resolve the demographic structure of corals, i.e., the relative composition of different stages or sizes. This is an important caveat because demographic changes are not necessarily reflected in changes in coral cover (Done 1995), so that impacts on a critical process (e.g., recruitment failure) may not be represented explicitly. Failure to identify which mechanisms (among partial or whole-colony mortality, recruitment, or colony growth; Hughes and Tanner 2000) are implicated in coral cover change limits our ability to predict coral trajectories (Edmunds and Riegl 2020). Moreover, stress-induced coral mortality is often size specific, and which size classes are affected will have important implications for the following rate of recovery. Accurate hindcast and forecast predictions of coral cover require

a mechanistic approach by which the processes of coral gains (recruitment, colony growth) and losses (partial and whole-colony mortality) are considered explicitly at the colony level to account for size-specific and density-dependent responses.

We developed a mechanistic model of coral metapopulations to assess the cumulative impacts of multiple stressors that have recently affected the GBR. The model simulates the fate of individual coral colonies across >3,800 individual reefs connected by larval dispersal while capturing some effects of water quality (suspended sediments and chlorophyll) on the early life demographics of coral and CoTS. A reconstruction of recent (2008–2020) coral trajectories across the GBR was performed from (1) the integration of mechanistic data into empirical relationships that underlie the demography of corals and CoTS; (2) the calibration of stress-induced coral mortality and recovery with observations from the GBR; (3) the simulation of coral dynamics under spatially and temporally realistic regimes of larval connectivity, water quality, CoTS outbreaks, cyclones, and mass coral bleaching; and (4) the validation of these trajectories with independent coral cover observations. We then combined statistical and simulation-based approaches to evaluate the relative contribution in space and time of each driver to the reconstructed reef response. Specifically, we asked (1) what are the individual and combined effects of acute stressors (cyclones, CoTS and bleaching) in terms of proportional coral loss across the GBR? (2) What is the relative importance of water quality and connectivity on recovery dynamics at both local and regional scales? (3) What are the reefs' abilities to sustain healthy levels of coral cover considering their spatial regimes of acute and chronic disturbances? Finally, we calculated the equilibrium state of coral cover of each reef, which integrates the cumulative pressures operating on coral population growth and stress-induced mortality. Specifically, we determined the net outcome of exposure to disturbances, resistance to such disturbances, and the rate of recovery. In practice, the disturbance-driven nature of reefs means that they will rarely maintain their "equilibrium state" but the measure is comparable among reefs and consistent with a general definition of resilience, that is a system's capacity to maintain functional levels of structure and processes in the face of disturbances (Gunderson and Holling 2002, Walker et al. 2006). With this mechanistic evaluation of cumulative impacts and reef resilience we attempt to elucidate the main drivers of coral reef decline and provide guidance for reef monitoring and targeted management to help sustain a healthy GBR.

MATERIALS AND METHODS

Model general description

ReefMod (Mumby et al. 2007) is an agent-based model that simulates the settlement, growth, and

mortality of circular coral colonies and patches of algae over a horizontal grid lattice. With a 6-month time step, the model tracks the individual size (area in cm^2) of coral colonies and algal patches affected by demographic processes, ecological interactions, and acute disturbances (e.g., storms, bleaching) characteristic of a mid-depth (~5–10 m) reef environment. The model has been successfully tested against *in situ* coral dynamics both in the Caribbean (Mumby et al. 2007, Bozec et al. 2015) and the Pacific (Ortiz et al. 2014, Bozec and Mumby 2019).

We developed the model further to integrate coral metapopulation dynamics across a spatially explicit representation of the multiple reef environments of the GBR (ReefMod-GBR, Fig. 1A, Appendix S1). We refined a previous parameterization of coral demographics (Ortiz et al. 2014) based on three groups of acroporids (arborescent, plating, and corymbose) and three non-acroporid groups, including pocilloporids, a mix of submassive/encrusting corals and large massive corals, using recent empirical data from the GBR (Appendix S2: Table S1). The model was extended with explicit mechanisms driving the early life dynamics of corals: fecundity, larval dispersal, density-dependent settlement, juvenile growth, and background (chronic) mortality, mediated by water quality and transient coral rubble. In addition, a cohort model of CoTS was developed to simulate the impact of starfish outbreaks on coral populations. Processes of coral recovery and stress-induced mortality were calibrated with regional data, leading to a realistic modeling of the key processes driving coral populations on the GBR (Fig. 1B, C). ReefMod-GBR is implemented using the MATLAB programming language.

Model domain and spatial context.—For simulating coral dynamics along ~2,300 km length of the GBR, we used a discretization of the GBR consisting of 3,806 individual reef patches (Hock et al. 2017) across the northern, central, and southern sections of the GBR Marine Park (Fig. 1A). A grid lattice of 20×20 cells, each representing 1 m^2 of the reef substratum, was assigned to every reef patch (hereafter referred to as a reef) identified by a convex polygon in the indicative reef (0–10 m) outline (GBRMPA 2007). Because larval dispersal and environmental forcing are not consistently available at intra-reef scales, each grid lattice represents a mean-field approximation of the ecological dynamics occurring within the environment of a defined reef polygon. This environment is characterized by historical events of tropical storm and heat stress, and a reconstructed regime of water quality during austral summer (wet season, from November to April) and winter (dry season, May to October). Within-reef variability of coral demographics is implicitly included through stochastic coral recruitment and mortality, but also temporally through probabilistic storm and heat stress events. Uncertainty in coral and CoTS trajectories is captured by running a

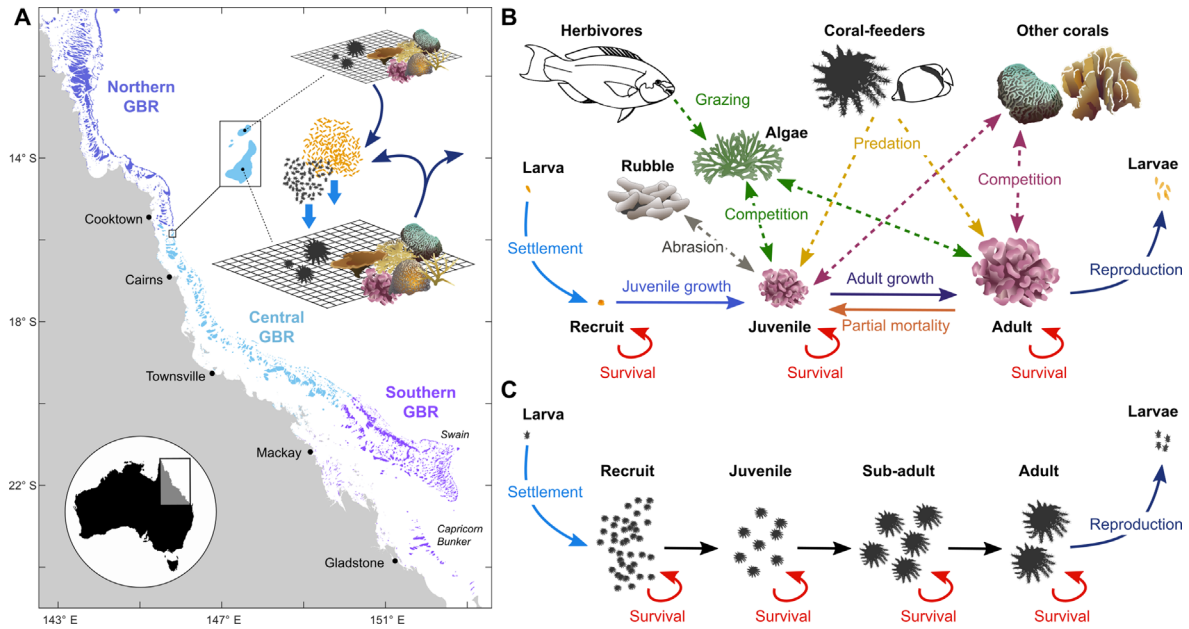


FIG. 1. Schematic representation of the reef ecosystem model applied to the Great Barrier Reef (ReefMod-GBR). (A) Each of 3,806 individual reefs is represented by a 20×20 m horizontal space virtually colonized by coral colonies belonging to six morphological groups. (B) Demographic processes (solid arrows) and ecological interactions (dashed arrows) affecting coral colonies individually. (C) Modeling of crown-of-thorns starfish (CoTS) cohorts subject to size-specific survival during their life. For both corals and CoTS, settlement occurs from a pool of larvae that results from the retention of locally produced offspring (self-supply) and the incoming of larvae from connected reef populations (external supply).

minimum of 40 stochastic simulations. As a result, the model is spatially explicit in three ways: (1) by simulating individual coral colonies on a representative reefscape, (2) by linking coral demographics to their ambient stress regime, and (3) by connecting reefs in a directed network that represents larval exchanges for both corals and CoTS.

Larval production and transport.—Broadcast coral spawning on the GBR extends from October to December (Babcock et al. 1986). Following Hall and Hughes (1996), coral fecundity is a function of colony size and expressed as the total volume of reproductive outputs (Appendix S1) using species-specific parameters (Appendix S2: Table S1). Colony size at sexual maturity was fixed to $123\text{--}134\text{ cm}^2$ for the three acroporid groups and $31\text{--}38\text{ cm}^2$ for the other groups, based on threshold sizes above which 100% of colonies were found reproductive (Hall and Hughes 1996). The number of offspring released by each coral group during the reproductive season is estimated by summing the total volume of reproductive outputs over all gravid colonies, assuming an average egg volume of 0.1 mm^3 (*Acropora hyacinthus*; Hall and Hughes 1996).

The CoTS spawning period on the GBR extends from December to February (Babcock and Mundy 1992, Brodie et al. 2017). CoTS fecundity expressed as number of eggs is a function of wet mass (Kettle and Lucas 1987) derived from the representative mean size (diameter) of

each age class of CoTS. The resulting fecundity-at-age prediction is multiplied by the density of the corresponding age class to calculate the total number of offspring produced on a grid lattice. Starfish become sexually mature when they are 2 yr old (Lucas 1984).

During a spawning season, the number of coral and CoTS offspring produced on each grid lattice is multiplied by the area of the associated reef polygon to upscale reproductive outputs to the expected population sizes. Larval dispersal is then processed from the reef of origin to destination reefs using transition probabilities representative of broadcast coral spawners (*Acropora* spp.) and CoTS larvae (Hock et al. 2017, 2019) derived from particle tracking simulations generated by a three-dimensional hydrodynamic model of the GBR (Herzfeld et al. 2016). These probabilities of larval connectivity are combined with the number of larvae produced to estimate larval supply on every destination reef. Matrices of larval connectivity were determined for designated spawning times for both corals and CoTS over the 6 yr for which the hydrodynamic models were available: wet seasons 2010–2011, 2011–2012, 2012–2013, 2014–2015, 2015–2016, and 2016–2017.

We note that local retention predicted by the connectivity matrices is extremely low for corals, as the relative proportion of coral larvae settling on the reef of origin is <0.01 for more than 95% of the 3,806 reefs. However, the empirical rates of larval retention for corals and CoTS across the GBR remain largely unknown. In a

study of coral recruitment around a relatively isolated reef of the central GBR, Sammarco and Andrews (1989) observed that 70% of the coral spats collected within a 5 km radius were found within 300 m of the reef. Assuming that ~40% of the produced larvae survive and become competent for settlement 8–10 d after spawning (Connolly and Baird 2010), a rate of 0.28 was considered as a minimum retention for both corals and CoTS and added to values predicted by dispersal simulations.

Larval supply and recruitment.—For a given reef, the total number of incoming coral and CoTS larvae (i.e., from external supply and retention) is divided by the area of the reef to estimate a pool of larvae L (larva/m²) available for settlement. Assuming density dependence in early (<6 month) post-settlement survivorship, we first estimate a density potential for settlers (D_{settlers} , settlers/m²) as a Beverton-Holt (B-H) function (e.g., Haddon 2011) of the available larval pool (L):

$$D_{\text{settlers}} = \frac{\alpha \times L}{\beta + L} \quad (1)$$

where α (settlers/m²) is the maximum achievable density of settlers for a 100% free space and β (larvae/m²) is the stock of larvae required to produce one-half the maximum settlement. For CoTS, the actual density of 6-month-old recruits is obtained by reducing D_{settlers} to a 3% survived fraction due to intense predation (Keesing and Halford 1992, Okaji 1996). For corals, the actual number of 6-month-old recruits for each coral group is generated in each cell separately following a Poisson distribution with recruitment event rate λ (recruit/m²) calculated as

$$\lambda = D_{\text{settlers}} \times A \quad (2)$$

where A is the proportional space covered by cropped algal turf on a given cell, i.e., the substratum that is suitable for coral recruitment (Kuffner et al. 2006). This assumes that the probability of coral recruitment is directly proportional to available space (Connell 1997). Corals cannot recruit on patches of ungrazable substrata, which are randomly distributed across the grid lattice at initialization (Appendix S1).

Recruitment parameters α and β were determined by calibration against GBR observations from offshore (mid- and outer-shelf) reefs. For corals (calibration for CoTS is presented thereafter), we simulated coral recovery on hypothetical reefs (see details in Appendix S1) and adjusted the two parameters with the double constraint of reproducing the recovery dynamics observed after extensive coral loss (Emslie et al. 2008; Fig. 2A) while generating realistic densities of coral juveniles (Trajon et al. 2013; Fig. 2B). Density patterns of coral juveniles varied predictably along the recovery curve: first, by increasing as self-supply of larvae is enhanced by more abundant sexually mature corals; second, by

decreasing with the progressive reduction of settlement space. Recovery dynamics will likely vary with external supply, water quality, and changes in coral community structure.

Early post-recruitment coral demographics.—Six-month-old coral recruits have a fixed size of 1 cm² and become juveniles at the next step if allowed to grow. Coral juveniles are defined by colony diameters below 4 cm. Their growth rate is set to 1 cm/yr radial extension (Doropoulos et al. 2015, 2016) until they reach 13 cm² (i.e., ~4 cm diameter, 2 yr old corals if no partial mortality has occurred) above which they acquire species-specific growth rate (Appendix S2: Table S1). With this parameterization, the maximum diameter of 3-yr-old corymbose/small branching acroporids is 10.1 cm, which falls within the range of diameters (7.8–13.7 cm) observed for *Acropora millepora* at this age (Baria et al. 2012).

Background whole-colony mortality of coral juveniles is set to 0.2 per year as recorded for *Acropora* spp. at Heron Island (Doropoulos et al. 2015). Corals above 13 cm² have escaped the most severe post-settlement bottlenecks (Doropoulos et al. 2016) and are subject to group- and size-specific rates of partial and whole-colony mortality (Appendices S1, S2: Table S1).

Effects of suspended sediments on early coral demographics.—River run-off exposes coral reefs to loads of sediments that are transient in space and time (Schaffelke et al. 2012, Waterhouse et al. 2017). These dynamics were captured from retrospective (2010–2018) spatial predictions of suspended sediments using the eReefs coupled hydrodynamic-biogeochemical model (Herzfeld et al. 2016, Baird et al. 2017). eReefs simulates the vertical mixing and horizontal transport of fine sediments across the entire GBR, including sediments entering the system through river catchments (Margvelashvili et al. 2018). We used the 4-km resolution model (GBR4) with the most recent catchment forcing (model configuration GBR4_H2p0_B3p1_Cq3b). Daily predictions of suspended sediment concentrations (SSC) were obtained by summing variables describing the transport and resuspension of small-sized particles: mud (mineral and carbonate, representative size 30 μm with a sinking rate of 17 m/d), which represent resuspending particles from the deposited sediments, and fine sediment (FineSed; 30 μm , sinking rate 17 m/d) and dust (1 μm , sinking rate 1 m/d), which come from river catchments.

Suspended sediments influence many aspects of coral biology (Jones et al. 2015) but are only considered here at the early life stages of broadcast spawning corals. Using published experimental data (Humanes et al. 2017a, b), we modeled dose–response curves between SSC (mg/L) and the success rate of various early life processes of corals: gamete fertilization, embryo development and subsequent larval settlement, recruit survival, and juvenile growth (Appendix S3: Figs. S1A–C).

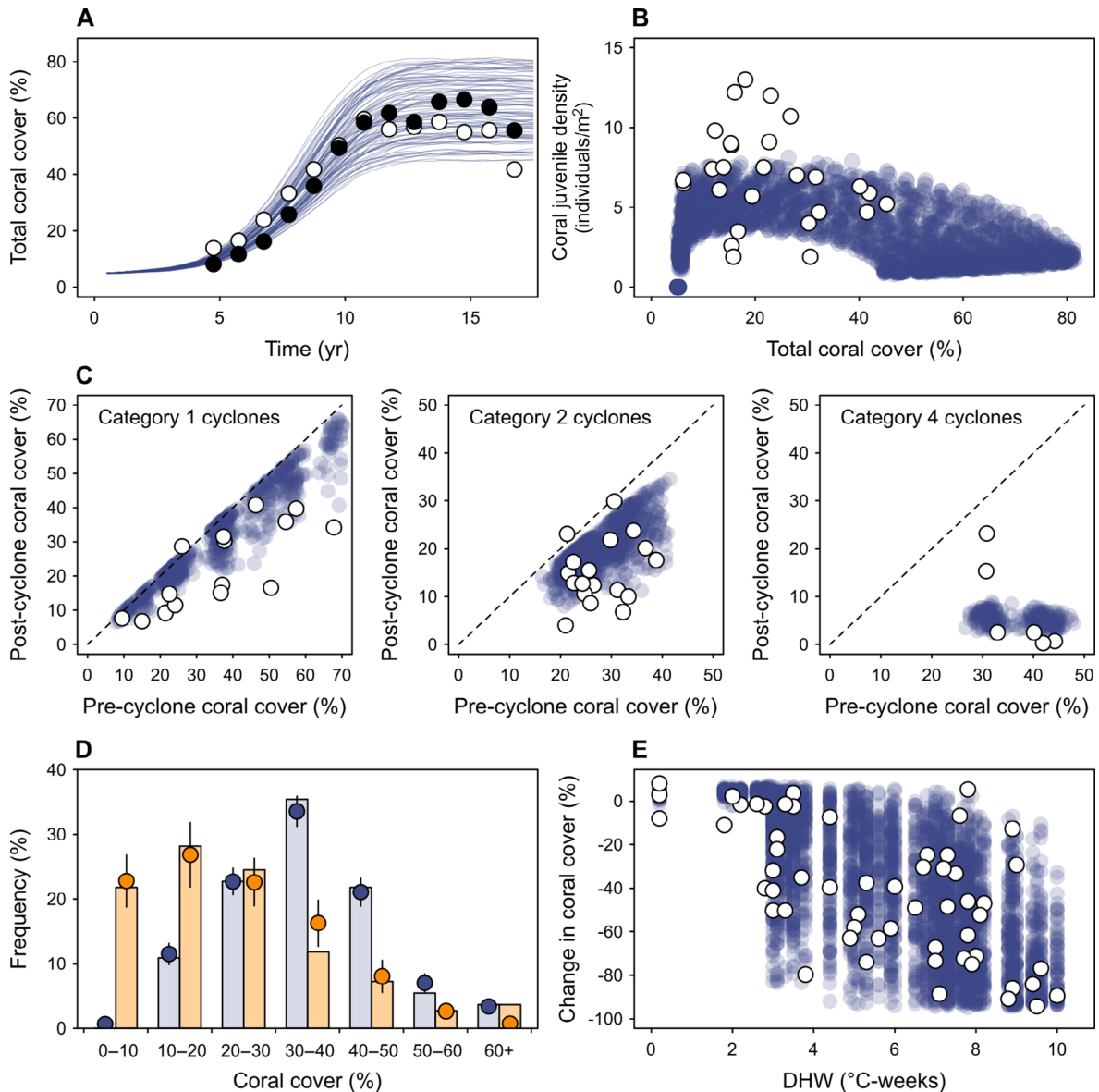


FIG. 2. Calibration of ReefMod-GBR. (A) Mean coral recovery trajectories (overlaid lines) for hypothetical reefs ($n = 40$) after calibration of coral recruitment parameters with observed recovery on the outer shelf of the northern (black dots) and southern (white dots) GBR (Emslie et al. 2008). (B) Resulting density of coral juveniles along the recovery trajectories compared with observations (Trapon et al. 2013) on the mid-shelf GBR (white dots). Juveniles are defined here as corals < 5 cm, excluding 6-month old recruits (~ 1 cm) for comparison. (C) Calibration of storm damages on AIMS LTMP sites (white dots, observations; blue dots, simulations; $n = 40$ stochastic runs) for the expected storm intensities (category 1, 2 and 4). Dotted lines indicate equality between pre- and post-disturbance coral cover (i.e., no change). (D) Frequency distributions of coral cover on 63 individual reefs before and after bleaching as measured (Hughes et al. 2018) across the GBR (blue and orange bars, respectively) and as simulated (blue and orange dots, respectively, $n = 40$ stochastic runs) after calibration of long-term bleaching mortality. (E) Corresponding coral cover changes in response to heat stress (degree heating weeks, DHW) as observed (white dots; Hughes et al. 2018) and simulated (blue dots, $n = 40$ stochastic runs of the 63 reefs). A minimum 3°C -weeks was assumed for bleaching mortality to occur.

Experiments and fitting procedures are detailed in Appendix S1.

Spawning corals release combined egg–sperm bundles that immediately ascend to the surface where fertilization and embryo development take place (Richmond

1997, Jones et al. 2015). To capture sediment exposure at these early (< 36 h) developmental stages, we extracted near-surface (-0.5 m) eReefs predictions of SSC at the assumed dates of mass coral spawning of six reproductive seasons (2011–2016). For each 4-km pixel, SSC was

averaged over 3 d following field-established dates of *Acropora* spp. spawning (Hock et al. 2019) in the northern, central, and southern GBR, then averaged among consecutive (split) spawning events (Appendix S3: Fig. S2). The resulting SSC values were assigned to the nearest reef polygon and used to predict, for each spawning season, the success of coral fertilization (Appendix S1: Eq. S10) and embryo development (manifested as subsequent larval settlement, Appendix S1: Eq. S11), which we combined to obtain an overall rate of reproduction success (Appendix S3: Figs. S1D, S3). The resulting rate can be multiplied by the number of coral offspring released before dispersal to simulate sediment-driven reductions in coral reproduction.

Daily predictions of SSC at 6 m depth from 2010 to 2018 (Appendix S3: Fig. S4) were used to predict the survivorship of *Acropora* recruits (Appendix S1: Eq. S12) and the growth potential of all juveniles (Appendix S1: Eq. S13). Recruit survivorship was expanded to a 6-month period by multiplying the daily survival rates over each summer (Appendix S3: Figs. S1E, S5). Juvenile growth potential was predicted from the SSC values averaged over each season (Appendix S3: Figs. S1F, S6, S7).

Impacts of cyclones on corals.—Cyclone-generated waves cause coral dislodgement and fragmentation. While the wave power needed to dislodge colonies of various sizes and shapes has been estimated (Madin et al. 2014), a measure of wave power at the scale of individual colonies is often unavailable. Indeed, work is underway to estimate coral loss from the duration of local exposure to cyclone-generated sea states capable of damaging reefs, as this can more readily be reconstructed than wave power. In the meantime, we approximated storm-induced colony mortality as a function of colony size and storm intensity defined on the Saffir-Simpson scale (1–5; Mumby et al. 2007, Edwards et al. 2011, see Appendix S1). Briefly, the probability of whole-colony mortality for the most severe storm (category 5) is assumed to be a quadratic function of colony size: small colonies avoid dislodgement due to their low drag, intermediate-sized corals have greater drag and are light enough to be dislodged, whereas large colonies are heavy enough to prevent dislodgement. A Gaussian-distributed noise $\epsilon \sim N(\mu = 0, \sigma = 0.1)$ adds variability to mortality predictions. For storm categories 1–4, these predictions are lowered by 95%, 88%, 75%, and 43%, respectively (Edwards et al. 2011, Appendix S1). Coral colonies larger than 250 cm² suffer partial mortality (i.e., fragmentation): the proportional area lost by a colony follows a normal distribution $N(\mu = 0.3, \sigma = 0.2)$ for a category 5 storm (Mumby et al. 2007), while the aforementioned adjustments are applied for other storm category impacts. Finally, scouring by sand during a cyclone causes 80% colony mortality in recruit and juvenile corals (Mumby 1999).

Because the above parameterization was initially derived for Caribbean reefs (Mumby et al. 2007, 2014, Edwards et al. 2011, Bozec et al. 2015), cyclone-driven mortalities were calibrated with GBR observations of storm damages using the benthic survey database of the Australian Institute of Marine Science (AIMS) Long-Term Monitoring Program (LTMP). We extracted coral cover data on reefs surveyed within one year of storm damages and estimated for each reef the expected cyclone intensity using the Database of Past Tropical Cyclone Tracks of the Australian Bureau of Meteorology (BoM; see details in Appendix S1). The magnitude of partial- and whole-colony mortality, adjusted to each coral group following the specific response observed in the corresponding taxa (Appendix S2: Table S1), was tuned until a reasonable match between the simulated and observed coral cover changes was found for the expected cyclone categories (Fig. 2C). While some growth forms may exhibit different size–mortality relationships (see Madin et al. 2014), differences in the simulated mortalities among coral groups reflect those observed in the field after storm impact.

Mass coral bleaching.—Widespread coral bleaching is assumed to be driven by thermal stress (Berkelmans 2002, Hughes et al. 2017, 2018). We used the Degree Heating Week (DHW, °C-weeks) as a metric of the accumulated heat stress to predict bleaching-induced coral mortality (Eakin et al. 2010, Heron et al. 2016). In an extensive survey of shallow (2 m depth) corals across the GBR during the 2016 marine heat wave, Hughes et al. (2018) recorded initial coral mortality (i.e., at the peak of the bleaching event) on reefs exposed to satellite-derived DHW (Liu et al. 2017). A simple linear regression model ($R^2 = 0.49, n = 61$) can be fit to the observed per capita rate of initial mortality, $M_{\text{BleachInit}}$ (%), as a function of local thermal stress (Appendix S3: Fig. S8)

$$M_{\text{BleachInit}} = \exp(0.17 + 0.35 \times \text{DHW}) - 1. \quad (3)$$

$M_{\text{BleachInit}}$ was used as the incidence rate for both partial and whole-colony mortality caused by bleaching, assuming they are correlated in their response to thermal stress. The resulting mortality incidences were further adjusted to each coral group (Appendix S2: Table S1) following reported species susceptibilities (Hughes et al. 2018). For a coral affected by partial mortality due to bleaching, the extent of tissue lost (Baird and Marshall 2002) was set to 40% of the colony area for small massive/submassive (observations on *Platygyra daedalea*), 20% for large massive corals (*Porites lobota*), and a minimal 5% for the three acroporid groups (*A. hyacinthus* and *A. millepora*) extended to pocilloporids due to morphological similarities.

Because Eq. 3 only captured initial mortality of the 2016 GBR heat wave, coral response over an entire bleaching event (i.e., including post-bleaching mortality) was determined by calibration with coral cover changes

reported in the following 8 months (Hughes et al. 2018). We initialized hypothetical reefs with the observed pre-bleaching values of coral cover (Fig. 2D) and simulated heat stress using the DHW values recorded in 2016 (Appendix S1). The overall magnitude of the resulting bleaching mortalities (i.e., $M_{\text{BleachInit}}$) was progressively increased until the predicted coral cover changes matched the observations (Fig. 2D, E).

Crown-of-thorns starfish outbreak dynamics.—Outbreak dynamics of the crown-of-thorns starfish (*Acanthaster* spp., CoTS) were simulated using a simple cohort model where starfish density is structured in 6-month age classes. The model integrates nutrient-limited larval survivorship and age-specific mortality, which are key for predicting outbreak dynamics (Birkeland and Lucas 1990, Pratchett et al. 2014).

Because the survival of pelagic-feeding CoTS larvae is strongly dependent on phytoplankton availability (Okaji 1996, Wolfe et al. 2017), high nutrients following terrestrial run-off, especially after intense river flood events, may have the potential to trigger population outbreaks (Brodie et al. 2005, Fabricius et al. 2010). A daily survival rate (SURV) of CoTS larvae can be estimated from the concentration of chlorophyll *a* (chl *a*, µg/L), a proxy of phytoplankton abundance (Fabricius et al. 2010, Appendix S3; Fig. S9)

$$\text{SURV} = \left[\frac{1}{1 + \left(\frac{1.07}{\text{chl } a} \right)^{2.91}} \right]^{1/22}. \quad (4)$$

We extracted subsurface (0–3 m) daily concentrations of total chl *a* predicted by eReefs during eight consecutive spawning seasons (December 2010–February 2018, Appendix S3; Fig. S10). For each 4-km pixel, the average daily survival (geometric mean) over a spawning season was extended to 22 d (duration of the developmental period; Fabricius et al. 2010) and assigned to the nearest reef polygon (Fig. 3A, Appendix S3; Fig. S11). Nutrient-enhanced larval survivorship on a reef was simulated by multiplying the predicted survival to the number of offspring released before dispersal.

After dispersal, larval supply to a given reef was converted into a number of settlers (Eq. 1) with parameters determined by calibration. The fate of newly settled CoTS was determined by age-specific rates of mortality sourced from the literature (Appendix S2; Table S2). To derive this mortality function, we first estimated daily mortality rates from the reported surviving fraction of CoTS individuals and the period of observations. A log-log linear model ($R^2 = 0.80$, $n = 8$) was then fitted to the resulting mortality-at-age estimates (Fig. 3B)

$$M = 91.23 \times A^{-0.57} \quad (5)$$

where M represents the monthly mortality rate (%) of CoTS at age A (month). In simulations, mortality-at-age

was converted to a 6-month equivalent ($1 - (1 - M/100)^6$) and applied to the corresponding age class at every step. The same mortality function was used for all reefs in the absence of reliable data on predation on CoTS. Maximum CoTS age was set to 8 yr (Pratchett et al. 2014) with 100% of individuals older than that dying due to senescence.

The amount of coral surface consumed by CoTS over a 6-month period was determined from published rates of consumption per individual size (starfish diameter) during summer and winter (Keesing and Lucas 1992) after representative size-at-age conversions (Engelhardt et al. 1999). As a result, CoTS substantially feed on corals from the age of 18 months+ (~150–200 mm diameter). The amount of coral surface consumed for each coral group was determined using empirically derived feeding preferences (De'ath and Moran 1998). While relative feeding proportions reflect a strong preference for the three *Acropora* groups (~75% of CoTS consumption), these are further adjusted to the proportion of each coral group currently available on a reef.

The density of coral-eating CoTS (18 months+) collapses due to starvation when the cover of all acroporids and pocilloporids drops below 5%. Although this allows reproducing the observed rapid decline of outbreaking CoTS when coral is depleted (Moran 1986), mass mortalities in high-density populations of *Acanthaster* can also be triggered by disease (Zann et al. 1987, 1990, Pratchett 1999) before significant coral damage occurs (Pratchett 2010). To capture this density-dependent process, an outbreaking CoTS population will collapse after a random time period drawn from a uniform distribution of 2–5 yr, which is the duration of most observed outbreaks (Moran 1986, Pratchett et al. 2014). A CoTS population is considered to be outbreaking when the density of 18 months+ starfish reaches 0.6 individuals/400 m² (Moran and De'ath 1992).

CoTS outbreak dynamics and associated impacts on corals were calibrated using observations from Lizard Island, northern GBR (Pratchett 2005, 2010). Starfish populations were initialized with the density-at-size recorded in October–December 1996 after appropriate size–age conversion (Engelhardt et al. 1999). Because the first observed starfish size class (diameter <15 cm) is likely underestimated by visual surveys (MacNeil et al. 2016), its density was deduced from the 15–20 cm class following mortality at the corresponding age. Recruit (0–6 month old starfish) density was set to zero as expected in winter. Here, CoTS populations were forced to collapse after 2 yr as observed (Pratchett 1999, 2005). Simulations reproduced the observed changes in CoTS density (Fig. 3C) and size distribution (Appendix S3; Fig. S12) after lowering the mortality of 2 yr+ (>20 cm) starfish (Fig. 3B). Maximum settlement rate (α) was fixed to 100 settlers/m², which, with the above adjustment of adult mortality, gives an adult population size of ~64 adults (>25 cm) per 400 m² reef area, similar to

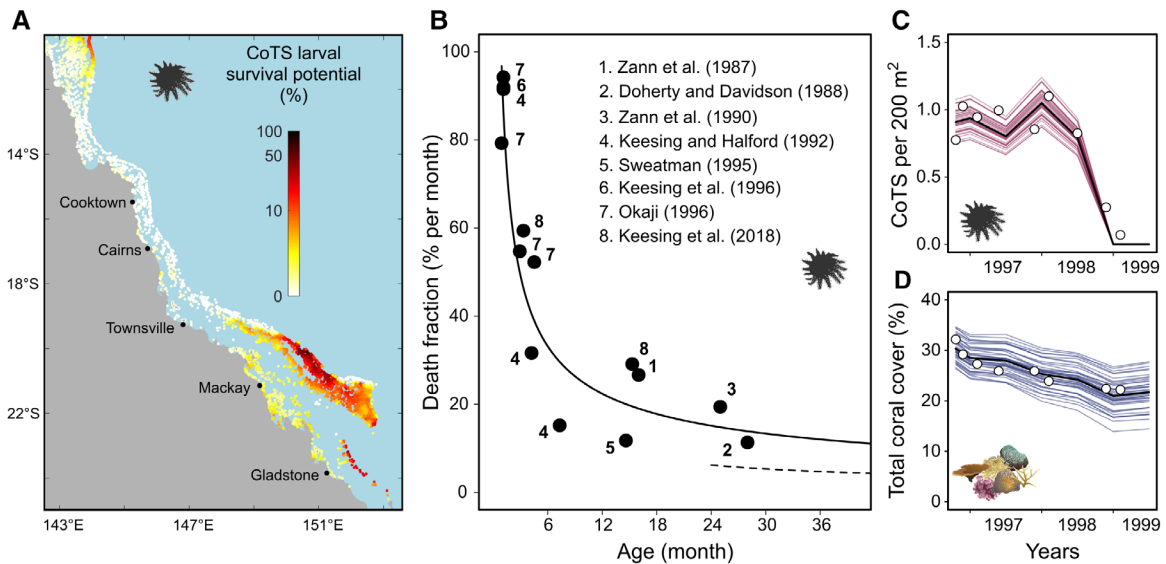


FIG. 3. (A) Percent survival rate of CoTS larvae before dispersal derived from subsurface (0–3 m) daily predictions (eReefs-GBR4) of chl *a* during the spawning season (December–February) averaged over the period 2010–2018. (B) Point estimates of CoTS mortality (monthly percent death fraction) as a function of individual age derived from manipulative experiments and cohort surveys (Appendix S1: Table S2) with the fitted log-log linear model ($\ln y = 4.51 - 0.57 \times \ln x$) equivalent to Eq. 5. Age was estimated as the median age of the cohort during the study period. Temporal changes in (C) CoTS densities and (D) coral cover as observed at Lizard Island (white dots; Pratchett 2005, 2010) and as simulated (colored lines, replicate trajectories; black lines, average trajectories) after calibration of mortality of 2 yr+ starfish (dotted line in B), coral consumption, and recruitment parameter β . Temporal changes in starfish size distribution (Appendix S3: Fig. S12) were also included in the calibration.

the maximum adult densities observed on the GBR (Engelhardt et al. 1999, 2001). The steepness of the B-H relationship (β) was set to 12,500 larva/m². Starting with the October–December 1996 average coral cover ($\mu = 30.7\%$, $\sigma = 0.2 \times \mu$, half being acroporids; Pratchett 2010), reproduction of the observed coral cover changes (Fig. 3D) required a near-doubling (1.8 \times) of the published feeding rates.

Unconsolidated coral rubble.—Coral mortality following acute stress generates loose coral debris that cover the reef substratum and inhibit coral recruitment (Fox et al. 2003, Biggs 2013). As a first approximation, we assume that the percent coral cover lost after disturbance converts into percent rubble cover, although collapsed coral branches might cover a larger area than their standing counterparts. Structural collapse occurs immediately after cyclones but is delayed for 3 yr after bleaching and CoTS predation (Sano et al. 1987). Coral juveniles do not survive on unconsolidated rubble (Fox et al. 2003, Viehman et al. 2018), which amounts to reducing their survivorship by the proportion of the reef area covered by rubble. Loose coral rubble tends to stabilize over time with processes of carbonate binding and cementation (Rasser and Riegl 2002). These dynamics were approximated using an exponential decay function (Appendix S3: Fig. S13) assuming that about two-thirds of coral rubble is consolidated after 4 yr (Biggs 2013).

Macroalgae and grazing.—The modeling of grazing and algal dynamics is detailed elsewhere (Bozec et al. 2019) so is only briefly described here. The model simulates algal dynamics by 1-month iterations using empirical rates of macroalgal recruitment and growth. Each grid cell can be occupied by four algal groups: (1) closely cropped algal turf (<5 mm), (2) uncropped algal turf (>5 mm), (3) encrusting fleshy macroalgae, and (4) upright macroalgae. Cropped algal turf is the default substratum maintained by repeated grazing onto which corals can settle and grow. When a cell is left ungrazed for 1 month, diminutive algal turf becomes uncropped and the two macroalgal groups grow following a logistic curve (Bozec et al. 2019). Considering that herbivorous fish are largely unexploited across the GBR (Smith et al. 2007), we set herbivore grazing to the maximum value, which results in macroalgae and turf being maintained in a cropped state suitable for coral settlement. Realistic spatial predictions of grazing levels are yet to be developed for the GBR and will require extensive data on the size structure and species composition of herbivorous fish across a range of habitats (Mumby 2006, Fox and Bellwood 2007).

Reconstruction of recent (2008–2020) reef trajectories of the GBR

Model simulations were run with spatially and temporally realistic regimes of water quality (SSC and chl *a*),

storms, and thermal stress to reconstruct the trajectory of coral cover of the 3,806 reefs between 2008 and 2020 (end of winter 2007 to end of winter 2020).

Initial coral cover on each reef was generated at random from a normal distribution $N(\mu, \sigma = 0.2 \times \mu)$ with mean value μ derived from AIMS monitoring surveys (Sweatman et al. 2008, Thompson et al. 2019) performed on 186 reefs between 2006 and 2008 (Appendix S1). Reefs that were not surveyed during this period were initialized with the mean coral cover of the corresponding latitudinal sector (11 sectors; Sweatman et al. 2008) and shelf position (inshore, mid-shelf, and outer shelf). Initial cover was generated for each coral group separately following the average community composition of each sector and shelf position. In the absence of reliable empirical estimates, random covers of loose coral rubble and ungrazable substrata were generated on each reef from a normal distribution $N(\mu, \sigma = 0.2 \times \mu)$ with mean value μ set arbitrarily to 10% and 30%, respectively.

The 2010–2018 regime of water quality (i.e., suspended sediments and chl *a*) predicted by eReefs was imposed as a recursive sequence over the 2008–2020 period. The same sequence was applied to the selection of connectivity matrices to preserve spatial congruence between larval dispersal and the hydrodynamic forcing of water quality. Past exposure to cyclones was derived from sea-state predictions of wave height (Puotinen et al. 2016). The potential for coral-damaging sea state (wave height >4 m) was determined using a map of wind speed every hour within 4-km pixels over the GBR for cyclones between 2008 and 2020. Any reef containing a combination of wind speed and duration capable of generating 4-m waves, assuming sufficient fetch, was scored as positive for potential coral-damaging sea state in the respective year. Where damaging waves were predicted, an estimate of cyclone category was deduced from the distance to the cyclone track extracted from the BoM historical database. To simulate past exposure to thermal stress, we extracted from the NOAA Coral Reef Watch (CRW) Product Suite version 3.1 (Liu et al. 2017) the 2008–2020 annual maximum DHW available at 5-km resolution, consistent with the DHW–mortality relationship of the 2016 bleaching (Eq. 3, Hughes et al. 2018). Reefs were assigned the maximum DHW value of the nearest 5-km pixel.

Exposure to *Acanthaster* outbreaks was hindcast by combining starfish demographic simulations with observed abundance from monitoring ($n = 289$ reefs with at least one survey between 2008 and 2020) conducted by the AIMS LTMP (Sweatman et al. 2008) and the Great Barrier Reef Marine Park Authority (GBRMPA) Reef Joint Field Management Program (GBRMPA 2019). Initial CoTS densities were predicted by hindcast (1985–2008) simulations of the Coral Community Network (CoCoNet) model (Condie et al. 2018). This predator–prey model simulated age-structured CoTS populations with fast- and slow-growing coral cover dynamics across ~3,000 reefs using a representative

regime of storms and bleaching ($n = 50$ stochastic runs). Mean densities of adult CoTS (as mean counts per hypothetical manta tow) predicted in 2008 were assigned to the 3,806 reefs and treated as rate parameter values of a Poisson distribution in order to initialize ReefMod with random CoTS densities. At the following steps, CoTS populations on reefs that were not surveyed in the respective year were predicted by population dynamics, whereas reefs surveyed that year were imposed the corresponding observation of adult count. Assuming 0.22 CoTS per tow represents 1,500 CoTS/km² (Moran and De'ath 1992), input count values were transformed into an equivalent starfish density per reef area and disaggregated by age following age-specific predictions of starfish mortality. Density-at-age was further corrected for imperfect detectability using empirical predictions from MacNeil et al. (2016).

The joint simulation of the 3,806 reef dynamics was replicated with 40 runs to capture demographic fluctuations emerging from stochastic initialization, recruitment, and mortality events. Regional mean values of coral cover were weighted by the log-transformed polygon area representative of each reef. Spatiotemporal patterns in the composition of functional groups were described for each region separately using correspondence analyses of the cover of the six coral groups per reef per year per run.

Model performance and functional sensitivity

To assess the ability of the model to reconstruct observed coral trajectories, predictions of total coral cover were compared to available time series from AIMS monitoring surveys (transects and standardized manta tows, Appendix S1). We selected $n = 95$ individual reefs monitored at least six times between 2009 and 2020 and compared visually the mean observed and predicted values of total coral cover over time. We also calculated the deviation between each predicted cover ($n = 40$) and the observed mean cover value of the corresponding time step in order to determine the distribution of prediction errors over each time series. We resampled coral cover values from the observed mean to generate a comparable amount of observations (i.e., 40 per monitoring survey) and computed the associated error distribution. The resulting distributions of prediction and observation errors were summarized by their 90% error intervals (i.e., range between the 5th and 95th percentiles) and compared visually for each monitored reef. Details of calculations are presented in Appendix S1.

In a similar manner to detection and attribution analyses in climate modeling studies (e.g., Bindoff et al. 2013), we ran a series of modeling experiments whereby each stressor is removed alternatively from the hindcast simulation to examine the resulting impact on the model fit to observations. Four hindcast scenarios were simulated (40 replicate runs each): (1) without cyclones; (2) without thermal stress; (3) without CoTS dynamics;

(4) without water-quality impacts on corals. For each alternative scenario, we reassessed the distribution of prediction errors along the reconstructed trajectories of the monitored reefs and computed the 90% error intervals per region and shelf position. By comparison to the baseline scenario (i.e., the hindcast with all stressors included), a shifted error interval toward positive errors would indicate that the missing stressor has a notable influence on the reconstructed trajectories (i.e., its exclusion leads to notable over-estimations of coral cover relative to the baseline). As such, this functional sensitivity analysis provides a first assessment of the respective influence of the different stressors on coral demographics across the monitored reefs.

Assessment of cumulative impacts and reef resilience during 2008–2020

To investigate temporal coral changes across the GBR, we quantified year-on-year absolute changes (AC) in percent coral cover for each reef

$$AC = C_{\text{fin}} - C_{\text{ini}} \quad (6)$$

where C_{ini} and C_{fin} are the percentage total coral cover at the beginning and at the end of a one-year period, respectively. Because the magnitude of coral cover change is likely dependent on the initial value of coral cover (Côté et al. 2005, Graham et al. 2011), we also calculated for every reef and every year the relative rate of coral cover change (RC) as follows:

$$RC = \frac{100 \times (C_{\text{fin}} - C_{\text{ini}})}{C_{\text{ini}}} \quad (7)$$

within one time-step of ReefMod simulation (i.e., 6 months), stress-induced coral mortality (i.e., due to CoTS, cyclones, and bleaching) is applied after the processing of coral recruitment, growth, and natural mortality. To quantify the individual impact of each of these stressors, their contribution to total coral cover loss was tracked annually and expressed both as absolute (% cover/yr) and relative cover loss (i.e., proportional to coral cover *before* disturbance, % per yr). The latter metric allowed calculation of standardized annual rates of coral mortality ($m_{r,s}$) on every reef r due to each stressor s (i.e., CoTS, cyclones, and bleaching), a necessary step for assessing the relative importance of the three acute stressors across the entire GBR.

To assess the potential of coral recovery, the absolute change in total coral cover over 6 months was extracted for each reef *before* stress-induced coral mortality, thus providing an estimate of total coral cover growth in the absence of disturbances. Spatial and temporal variations of these rates of coral community growth (g , in % cover/6 months) were analyzed with generalized linear models (GLM). Simulated data of the first two time steps were excluded to reduce the influence of model initialization.

Using GLMs as tools of variance partitioning for simulated data sets (White et al. 2014), we estimated the variance components of g per reef ($n = 3,806$) \times time step ($n = 24$) \times run ($n = 40$) explained by eight environmental variables: total coral cover before growth; cover of ungrazable substrata; cover of loose coral rubble; water-quality-driven percentage success of coral reproduction, recruit survival of acroporids, and juvenile growth; relative proportion of external vs. internal (self) larval supply in the connectivity matrices, where external supply is the sum of the connection strengths from source reefs; and number of connections from source reefs. The cover of coral rubble was time averaged for each reef \times run because its fluctuations and associated effects on coral juveniles are unlikely to impact coral cover over 6 months. For the same reason, the reef-specific values of water quality and connectivity variables were averaged over time. Residuals were modeled with a gamma distribution with a log link function. Because g can be negative (i.e., when natural mortality exceeds recruitment and colony growth) with a minimal value of -1.5% cover/6 months, it was fitted as $g + 2$ to obtain a strictly positive response variable.

The GLM predictions of g for a given reef environment can be used to simulate a stepwise process of coral cover growth using a simple recursive equation

$$C_{r,t} = C_{r,t-1} + g(C_{r,t-1}, P_{x,r,t-1}) \quad (8)$$

where the incremental growth of total coral cover (g) on reef r at step t is predicted from the previous-step value of coral cover ($C_{r,t-1}$) and the other environmental predictors ($P_{x,r,t-1}$). To assess the influence of water quality on coral recovery on inshore reefs, we simulated coral growth curves from an initial 5% cover using Eq. 8 and the percentage success of early life coral demographics calculated from representative steady-state (i.e., time-averaged) SSC values. The other predictors (ungrazable substrata, coral rubble, and connectivity drivers) were set to their median value. Finally, to visualize the recovery potential across the entire GBR, we mapped the standardized annual growth rate of every reef obtained by simulating Eq. 8 over two time-steps (i.e., yearly), from a hypothetical 10% coral cover and with the reef-specific values of water-quality and connectivity predictors.

Assessing the cumulative impacts of multiple stressors requires integrating both their acute and chronic effects on coral mortality and growth. This was performed by simulating coral cover in every reef as a dynamic balance between cover growth g and the combined rates of annual mortality $m_{r,s}$ due to CoTS, cyclones, and bleaching

$$C_{r,t} = [C_{r,t-1} + g(C_{r,t-1}, P_{x,r,t-1})] \times \prod_s (1 - m_{r,s}). \quad (9)$$

With this formulation, coral cover on a given reef has a single stable equilibrium (i.e., independent of initial

cover), which is fully determined by the adverse effects of growth and stress-induced mortality. This equilibrium state approximates the value of coral cover that would be obtained when averaged over a long period of time, provided that the regimes of recovery and disturbance remain unchanged.

The equilibrium cover of each reef was determined based on the associated forcing of water quality, larval connectivity, cyclones, bleaching, and CoTS. Although the 2010–2018 fluctuations of SSC can be considered as a near-typical regime of water quality, episodic storms and marine heat waves experienced between 2008 and 2020 may not adequately represent average exposures. We thus gathered additional data to extend the cyclone and bleaching regimes and calculate more reliable annual mortalities. For cyclones, we used simulated regimes of region-scale occurrence of storm categories that combine GBR historical statistics (1970–2011) with synthetic cyclone tracks (Wolff et al. 2018). For bleaching, we extended the NOAA time series of annual maximum DHW back to 1998 to capture earlier (i.e., 1998, 2002) mass bleaching on the GBR (Berkelmans et al. 2004, Hughes et al. 2017). From these historical rates of disturbances, we generated 100 stochastic scenarios of storm and bleaching events over 20 yr for every reef and inferred the associated mortality (relative coral cover loss) from regression models derived from the 2008 to 2020 reconstruction (Appendix S3: Fig. S14). The predicted coral losses were averaged across all scenarios to generate mean annual mortalities for each reef. For CoTS, we used the mean annual mortalities of the 2008–2020 reconstruction. Eq. 9 was simulated until a

near-equilibrium cover was achieved for each reef, and the resulting equilibrium states used as a metric quantifying the ecosystem potential of reefs under their cumulative stress regime of cyclones, bleaching, CoTS, and water quality. This metric allows for a comparative evaluation of reef resilience, which we define here as the capacity of individual reefs to maintain functional levels of coral cover over decadal time scales.

RESULTS

Reconstructed 2008–2020 reef trajectories

Hindcast simulations of 3,806 reefs (Fig. 4A) indicated an overall decline of corals during the period 2008–2020 with a reef-wide mean coral cover that dropped from ~29% to ~19% (annual absolute cover loss -0.74% cover/yr over 13 yr). This is equivalent to a 33% relative loss of the initial cover. There was considerable variation among the three regions in the annual rate of coral cover change (Table 1) due to geographic differences in the timing and magnitude of coral mortality events and recovery periods. Overall, simulated coral populations in the northern, central and southern regions declined by -15.2% , -2.9% , and -8.6% absolute cover, respectively. This corresponds to a relative loss of the initial cover of 54%, 13%, and 26% in each respective region. Cross-shelf variability in simulated reef trajectories was important (Appendix S3: Fig. S15) with the strongest relative losses obtained for the inner-shelf (63–73%), the northern mid-shelf (58%), and southern outer-shelf (44%) regions (Appendix S2: Table S3).

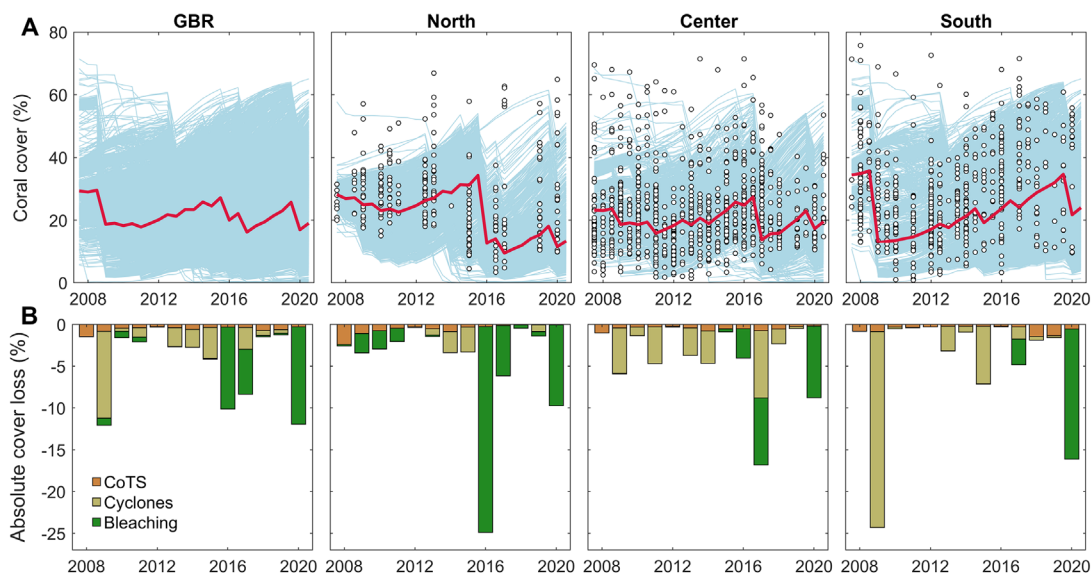


FIG. 4. (A) Hindcast (2008–2020) reconstruction of coral cover trajectories (blue lines, individual reef trajectories averaged over 40 simulations; red line, regional average for the whole GBR ($n = 3,806$ reefs) and the northern ($n = 1,201$ reefs), central ($n = 957$ reefs), and southern ($n = 1,648$ reefs) regions. Data points indicate observations of coral coverage from AIMS monitoring (transect and transformed manta tow estimates, Appendix S1). (B) Mean annual absolute loss of coral cover due to CoTS, storm damages and heat stress during 2008–2020.

TABLE 1. Mean annual rates (% cover/yr) of absolute coral cover change (AC), growth, and mortality from disturbances (crown-of-thorns starfish [CoTS], cyclones, and bleaching) for 2008–2020.

Parameter	GBR	North	Central	South
Net annual cover change	−0.7	−1.2	−0.2	−0.7
Annual cover loss				
Due to CoTS	−0.4	−0.4	−0.4	−0.5
Due to cyclones	−1.9	−0.6	−2.3	−2.9
Due to bleaching	−2.5	−4.0	−1.7	−1.6
Total	−4.9	−5.0	−4.5	−5.0
Annual growth	+4.1	+3.8	+4.2	+4.3

Notes: Growth represents the net outcome between coral cover growth (due to recruitment and colony extension) and natural mortality in the virtual absence of disturbances (formally, before disturbances occur). GBR, Great Barrier Reef.

The multivariate analyses of coral community composition over time and per region (Appendix S3: Fig. S16) revealed cross-shelf differences in the contribution of functional groups to total coral cover. Inshore reefs were mostly dominated by the group of mixed submassive/encrusting corals, whereas the functional composition of outer reefs was generally dominated by acroporids. Mid-shelf composition differed by region. Distinct patterns of community change emerged between periods of recovery and disturbance years, where composition abruptly diverged due to repeated losses of acroporids.

Model validation and sensitivity

At the reef level, the reconstructed coral trajectories generally matched field observations from monitoring data (Fig. 5) including the magnitude of observed coral declines following acute disturbances and the post-disturbance timing of coral recovery. Among the 95 monitored reefs selected to validate model predictions (Appendix S3: Fig. S17), 50% exhibited a mean predicted error (i.e., averaged over the time series) between −7.8% and +4.1% coral cover (Appendix S3: Fig. S18). Reefs of the northern GBR (cross-shelf) and on the outer-shelf of the central GBR exhibited the most accurate reconstructions. Coral cover was generally underestimated on mid-shelf reefs monitored in the central and southern regions, mostly due to over-predicted exposure to TC Hamish in 2009. Conversely, impacts of the same cyclone tended to be underestimated on outer reefs monitored in the southern GBR.

When compared to the baseline reconstruction (i.e., hindcast with all stressors included) of monitored reef trajectories, the alternative scenario without cyclones had the greatest impact on prediction errors in all regions (Fig. 6), indicating the importance of integrating cyclone damages for predicting coral cover across the GBR. The next important stressor was heat stress despite a lack of monitoring data after the 2020 marine heat wave. Water quality was the least influential stressor on prediction errors, even for reefs monitored inshore.

Coral loss due to bleaching, cyclones, and CoTS

There were considerable variations in the magnitude of simulated coral loss across years and among the three regions (Fig. 4B). Averaged over the 2008–2020 period and across the entire GBR (Table 1), bleaching was the most important driver of coral loss (−2.5% cover/yr mean annual absolute cover loss) followed by cyclones (−1.9% cover/yr), well ahead of CoTS (−0.4% cover/yr). The three stressors resulted in a cumulative annual loss of −4.9% cover/yr throughout the GBR, with the northern and central regions being the most and least affected, respectively.

Simulated impacts of bleaching essentially occurred during the last 5 yr, with intense and widespread heat stress (Fig. 7A) causing an estimated mean absolute decline of −9.8% cover in 2016, −5.5% cover in 2017, and −11.8% cover in 2020 throughout the entire GBR (Table 2, Fig. 7B). The 2020 heat wave produced the most severe impacts in terms of proportional coral loss (40% mean loss of pre-bleaching coral cover, Table 2) and number of impacted reefs (85% of reefs with a proportional loss >20%; 2016, 39%; 2017, 45%, Fig. 7C). The Northern GBR was the most severely impacted sector with all three bleaching events causing significant coral loss, especially during 2016 (mean absolute loss of −24.6% cover). The central region was also affected by the three heat waves, experiencing increasing levels of coral mortality at each bleaching event. While escaping mass bleaching in 2016, the Southern GBR was hit by the two following heat waves, especially in 2020 (−15.9% cover). Overall, only 10% of the GBR experienced >20% proportional loss for all three events of mass bleaching. Spatial discrepancies between the footprint of heat stress and absolute cover loss (e.g., in the far north in 2017 and 2020) were likely caused by prior coral depletion, leading to a decoupling between absolute (Fig. 7B) and proportional cover loss (Fig. 7C) in these regions.

While the simulated cyclones during 2008–2020 had relatively minor impacts across the Northern GBR, they were an important driver of coral loss in the central and southern regions (Fig. 4B, Table 1). In particular, TC Hamish in 2009 caused considerable impacts across the Southern GBR with an average loss of −22.5% cover (65% proportional cover loss), making it the most catastrophic disturbance event at a regional level during 2008–2020 (Appendix S2: Table S4). Other notable storm events included TC Yasi in 2011 (Central GBR), Ita in 2014 (Northern/Central GBR), Marcia in 2015 (Southern GBR), and Debbie in 2017 (mainly Central GBR). Overall, 26% of the GBR experienced less than 20% proportional loss for all individual storm events.

Simulated impacts of CoTS outbreaks were of similar magnitude in the three regions in terms of annual absolute cover loss (between −0.4% and −0.5% cover/yr, Fig. 4B, Table 1). Because the magnitude of coral loss is dependent on initial reef states, the spatial comparison of stressor impacts requires expressing them as

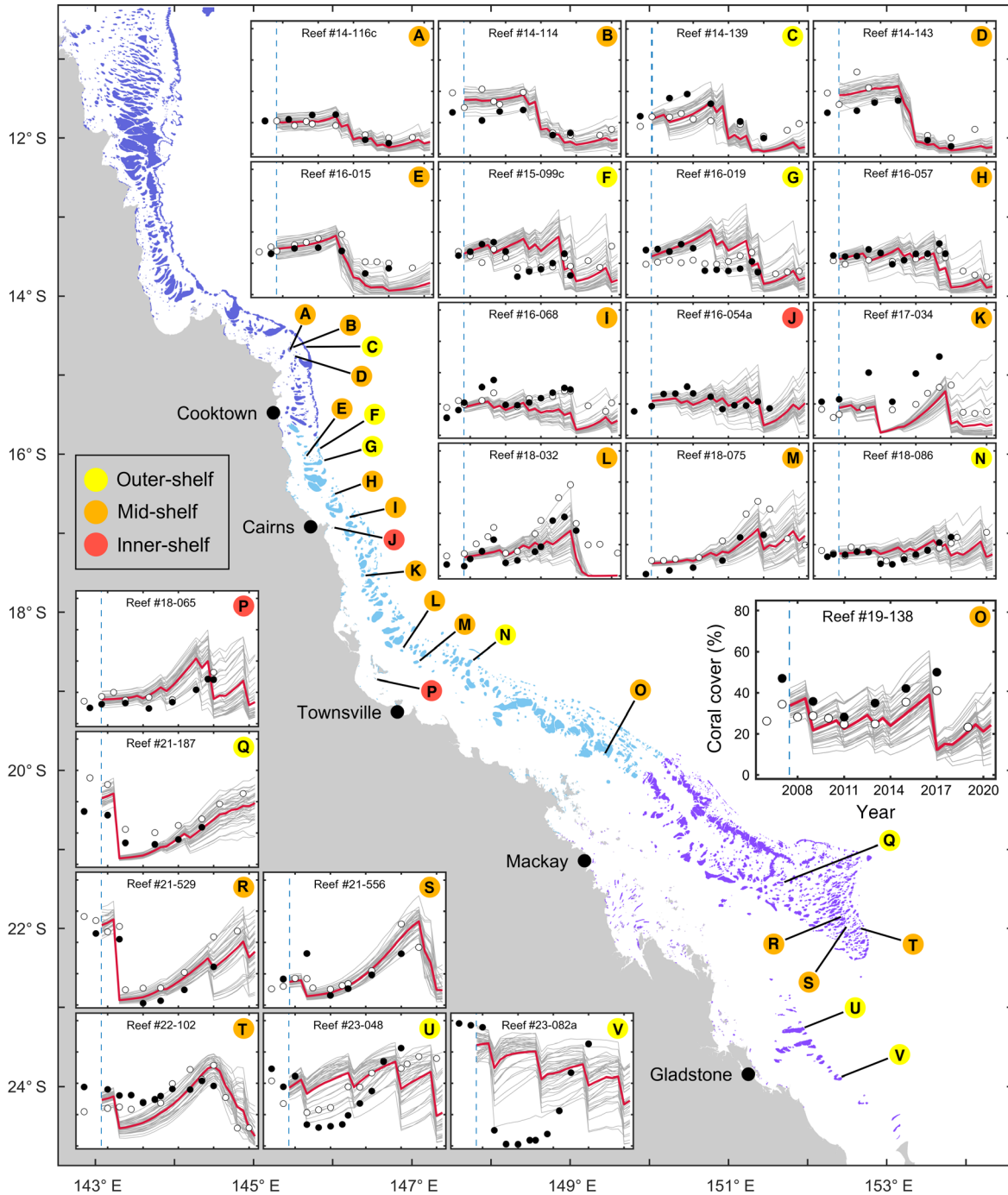


FIG. 5. Validation of the reconstructed trajectories of coral cover at the reef level (gray lines, individual trajectories; $n = 40$ simulations; red line, average trajectory) with field observations from AIMS monitoring programs (filled circles, point-intercept transects; open circles, standardized manta tows, Appendix S1). The dashed blue line indicates model initialization (winter 2007), whereby initial coral cover was determined as the mean cover of surveys performed between 2006 and 2008. Reefs selected for validation ($n = 22$) gathered at least six surveys during 2009–2020 (see Appendix S3: Fig. S17 for a broader selection of surveyed reefs). Panel O shows axis labels and values for inset panels A–V.

proportional losses relative to the pre-disturbance coral cover (Figs. 8A–C). Across the GBR, CoTS, cyclones, and bleaching caused, respectively, a mean 1.8%, 7.1%, and 8.5% proportional reduction of total coral cover

each year (Fig. 8D). Annual proportional cover loss revealed regional differences with greater CoTS impacts in the Central GBR (2.4%/yr) than in the northern (1.7%/yr) and southern (1.7%/yr) regions. At a reef scale,

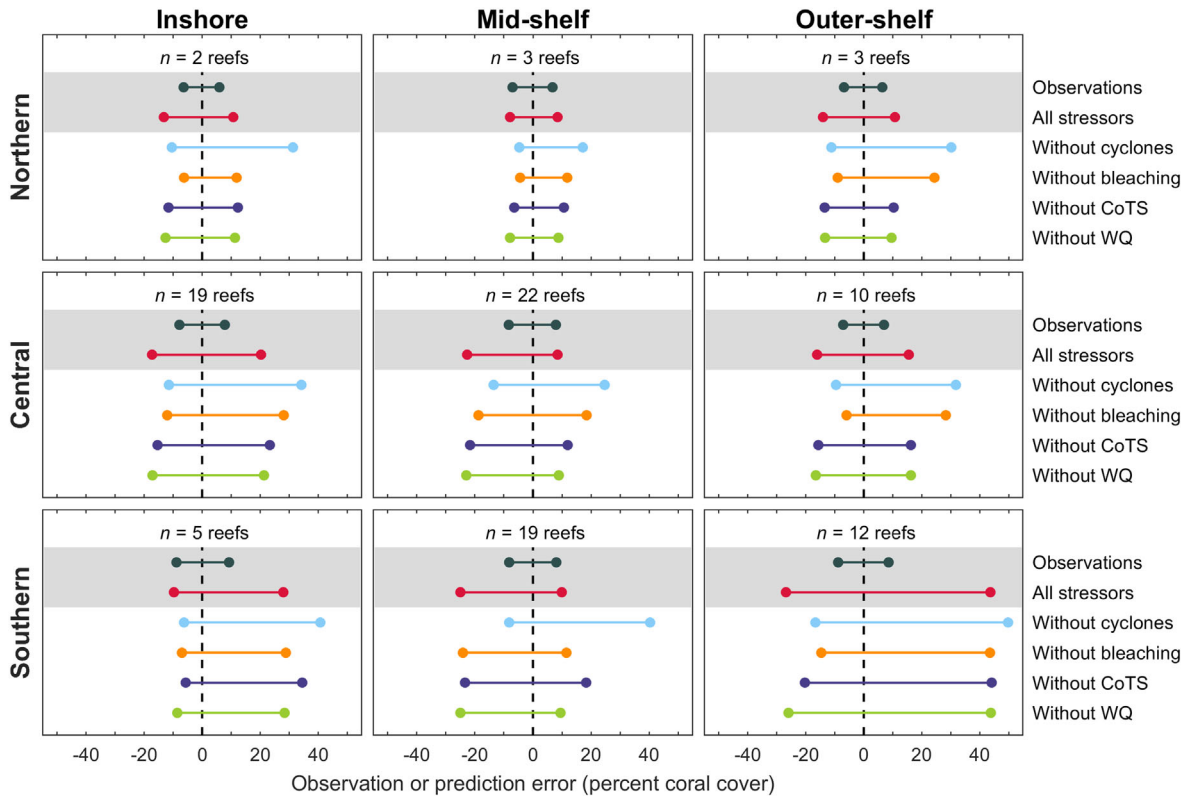


FIG. 6. Functional sensitivity analysis on the reconstructed coral trajectories of 95 reefs surveyed by AIMS monitoring programs. For each region, the 90% error intervals of observations and model predictions (Appendix S1) are represented to visualize the quality of model fits across multiple scenarios whereby each stressor is removed alternatively from the hindcast simulation.

relative impacts of CoTS outbreaks were extremely patchy with severe coral mortality (>15% per yr) occurring globally in the Cairns–Cooktown area (15° S–18° S) and at the southern end of the GBR (Figs. 8A, D). The distribution of storm impacts (Figs. 8B, D) revealed a region of intense coral cover mortality (>15% per yr) between 19° S and 21° S due to recurrent storm events (five to six storms between 2008 and 2020) with some particularly severe (TC Hamish in 2009 and Marcia in 2015). Bleaching-induced mortality increased from south to north and was generally stronger (>15% per yr) on the outer reefs (Figs. 8C, D).

Coral recovery potential

Subtracting total annual cover loss from net annual cover change (Table 1) allowed calculating an average rate of coral cover growth for each region: ranging from +3.8% to +4.3% cover/yr. Simulated coral community growth (g) over 6 months, extracted reef by reef before the processing of acute disturbances, was analyzed with GLMs fitted separately with every environmental predictor to assess their relative contribution on coral recovery (Appendix S2: Table S5). Total coral cover was, by far, the most important predictor of subsequent cover growth (25.0% deviance explained when fitted

alone), evidenced by a quadratic influence on g (Fig. 9 A). Other influential factors were the cover of ungrazable substrata (3.2% deviance explained), with a negative effect on coral cover growth intensifying as total coral cover increases (Appendix S3: Fig. S19A), and the three water-quality-driven demographic potentials (0.5–0.7%), which enhance coral cover growth as they achieve their full potential under low SSC (Appendix S3: Fig. S19B–C). The relative influence of the water-quality drivers on coral recovery increased when the GLMs were fitted on inshore reefs only (2.1%–3.8%, vs. 5.7% and 4.2% for coral cover and ungrazable cover, respectively), with the percentage success of coral (i.e., *Acropora*) recruitment being the prominent factor. Rubble cover and the two connectivity variables (proportion of external supply and number of external links) were the least influential factors on coral recovery. In total, the eight environmental drivers accounted together for 35.6% of the deviance explained by a global GLM fitted on all reefs.

Simulating coral cover growth curves from a recursive equation (Eq. 8) where growth is predicted by the global GLM revealed the impact of SSC on recovery dynamics on inshore reefs (Fig. 9B). From an initial 5% coral cover, growth predictions led to ~50% coral cover after ~10 yr under steady-state (year-averaged) SSC < 0.3

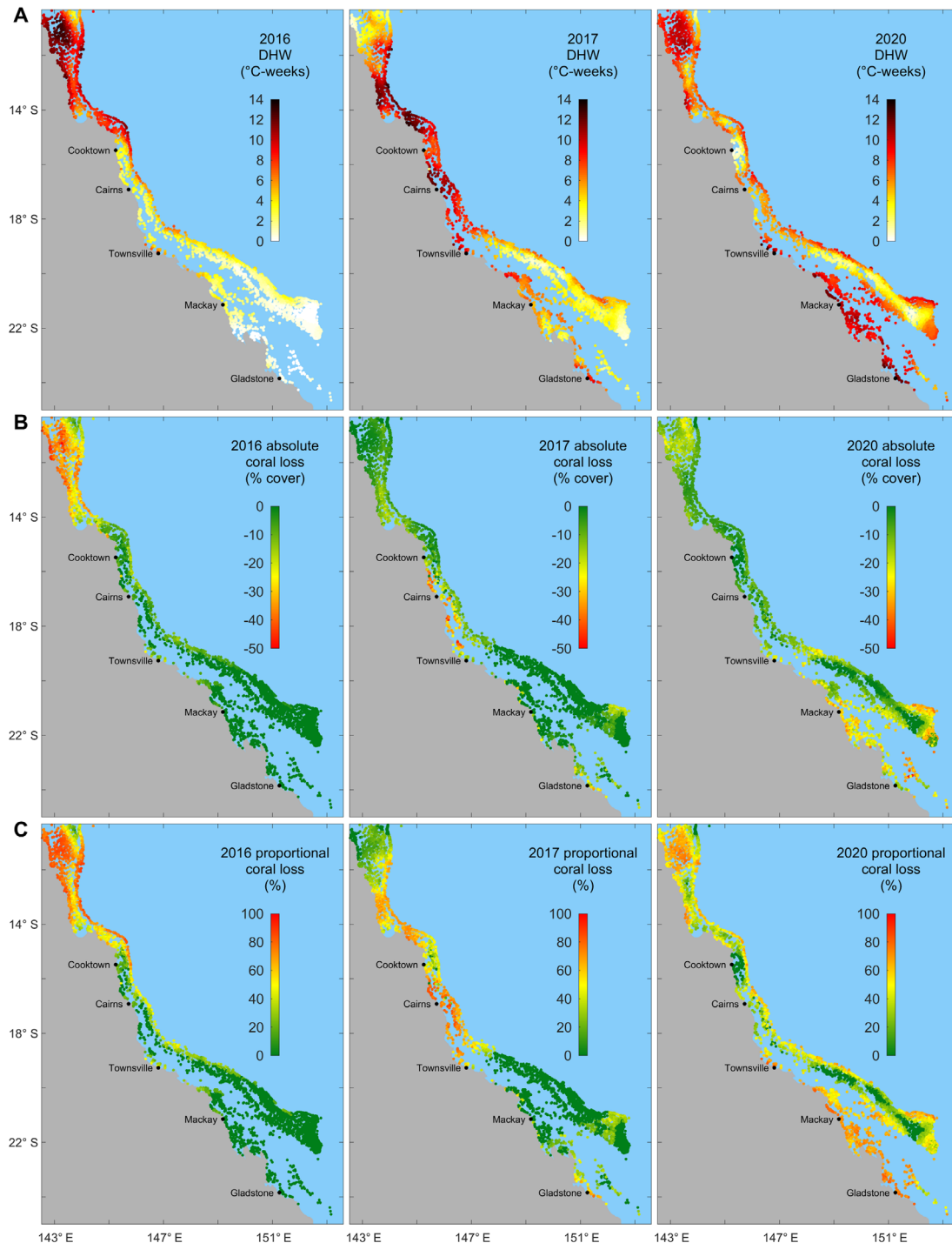


FIG. 7. Marine heat wave (2016, 2017, and 2020) associated predictions of reef-level (A) heat stress (seasonal maximum DHW), (B) absolute loss of total coral cover and (C) proportional loss (i.e., relative to pre-bleaching total coral cover) averaged over $n = 40$ simulations.

mg/L, a concentration that corresponds to the 10th percentile of inshore reefs ($n = 1,374$). Under steady-state $SSC > 4.5$ mg/L (75th percentile), the same level of coral cover (i.e., 50% cover) would be achieved after a

minimum of 15 yr, equivalent to a 50% increase in recovery time. Recovery to 50% coral cover was delayed by ~ 9 months for every 1 mg/L increment of steady-state SSC (inset, Fig. 9B).

TABLE 2. Impacts of the three marine heat waves (2016, 2017, and 2020) as absolute (percent cover) and proportional (in parenthesis) coral cover loss (i.e., relative to pre-bleaching total coral cover) averaged by region.

Year of mass bleaching	GBR	North	Central	South
2016	-9.8 (26%)	-24.6 (63%)	-3.5 (12%)	-0.1 (0%)
2017	-5.5 (24%)	-6.2 (37%)	-8.1 (29%)	-3.1 (8%)
2020	-11.8 (40%)	-9.6 (46%)	-8.7 (33%)	-15.9 (39%)

Note: Bleaching impacts result from reef-level predictions of heat stress (degree heating week [DHW]) and simulated coral community composition.

Cumulative impacts and reef resilience

The mapping of the standardized growth rate of total coral cover predicted by the GLM from 10% coral cover and reef-specific values of the environmental drivers revealed the geographic footprint of water quality (Fig. 10A). On average, the recovery potential was 14% lower inshore than offshore. On offshore reefs, the slowest growth rates were obtained in the Cairns–Cooktown region (14° S–18° S).

The combined rates of annual mortalities due to CoTS, cyclones, and bleaching (Fig. 10B), calculated using longer-term exposures to storms (1970–2011) and heat stress (1998–2020), revealed two regions of high coral mortality (up to 25% per yr): on the mid-shelf reefs of the Cairns–Cooktown region (14° S–18° S) and on the southern inshore (near Gladstone) and offshore reefs. Reefs with minimal total mortality were mostly found offshore between 20° S and 22° S.

The cumulative impacts of all stressors were reflected in the computed equilibrated covers (Fig. 10C), which approximate the average value of total coral cover under local regimes of water quality, CoTS, cyclones, and bleaching (Eq. 9). Equilibrated covers were obtained by simulating reefs individually over 100 yr to ensure they all achieved their deterministic equilibrium (Appendix S3: Fig. S20). The median equilibrium state was 45% coral cover on inshore reefs and 61% offshore (i.e., mid- and outer-shelf combined), reflecting the impact of water quality in the modeled coral dynamics.

DISCUSSION

Coral populations on the GBR are distributed over a vast network of disparate reef environments, making it extremely difficult to assess the relative contribution of multiple stressors in time and space. We developed a simulation model of coral demographics to quantify the cumulative effects of multiple disturbances and explain how they drive coral cover at local and regional scales. The model integrates existing knowledge on the core underlying mechanisms of coral population dynamics with state-of-the-art spatial data capturing fine-scale environmental forcing across >3,800 reefs. Our simulation of coral colony-scale processes under a temporally and spatially realistic stress regime provided a credible reconstruction of recent (2008–2020) trajectories of coral cover. Overall, the model indicated a general decline of coral cover over the past 13 yr, with mass coral bleaching and cyclones dominating the simulated share of total acute stress on the GBR. The model disentangled the

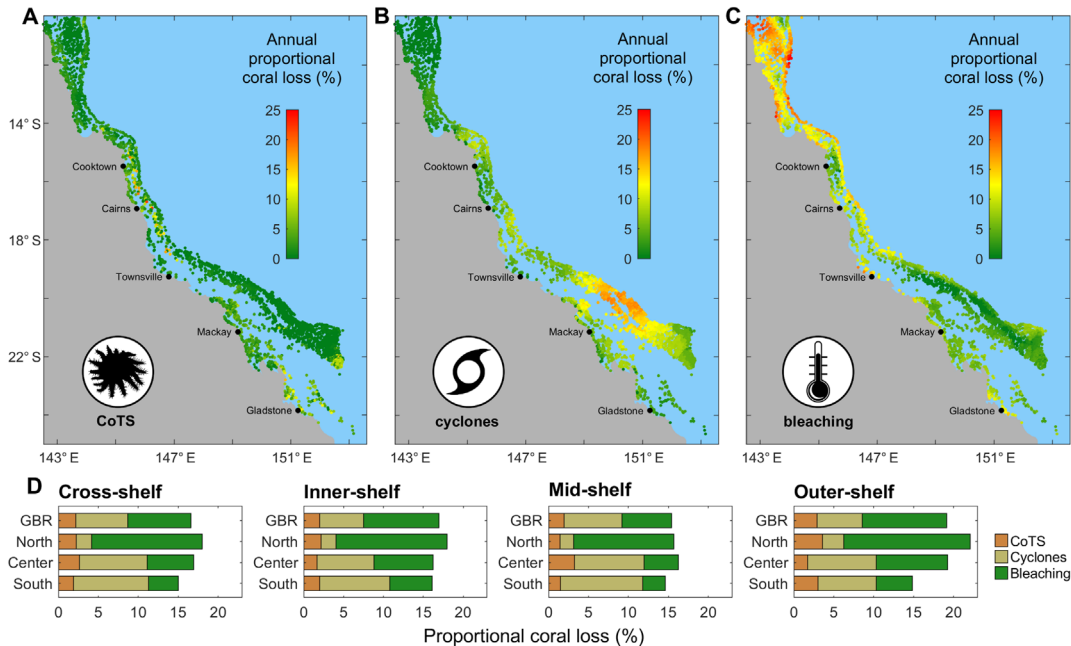


FIG. 8. The 2008–2020 mean annual proportional loss of coral cover across the GBR caused by (A) CoTS consumption, (B) cyclone damages, and (C) heat stress. (D) Mean annual relative cover loss per shelf position across the GBR.

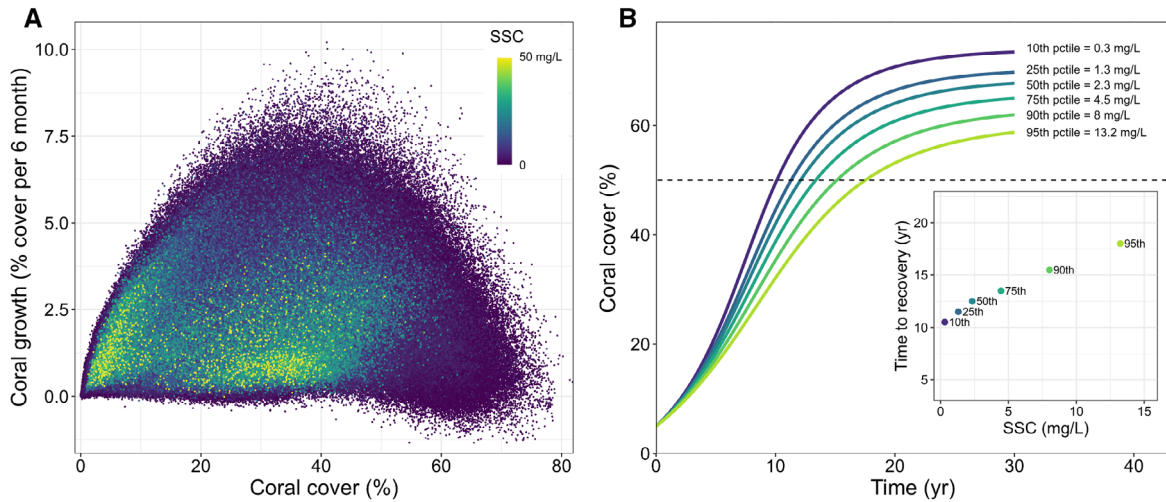


FIG. 9. (A) Quadratic influence of initial total coral cover on subsequent coral cover growth rate (g) on all reefs during 2009–2020 ($n = 3,653,760$ model realizations). Color codes to the predicted concentration of suspended sediment (SSC) averaged across all available years. (B) GLM-based coral recovery curves for hypothetical inshore reef environments exposed to year-round SSC (mg/L), obtained by the recursive prediction of g (Eq. 8) from an initial coral cover of 5%. The three water-quality drivers were calculated for representative SSC values of inshore reefs (10th, 25th, 50th, 75th, 90th, and 95th percentiles [ptile] out of 1,374 reefs) with the other predictors set to their median value (GBR-wide across all years): ungrazable, 30%; rubble, 11%; connect_{num}, 8.5; connect_{prop}, 0.06. The inset displays recovery times to 50% cover under each SSC.

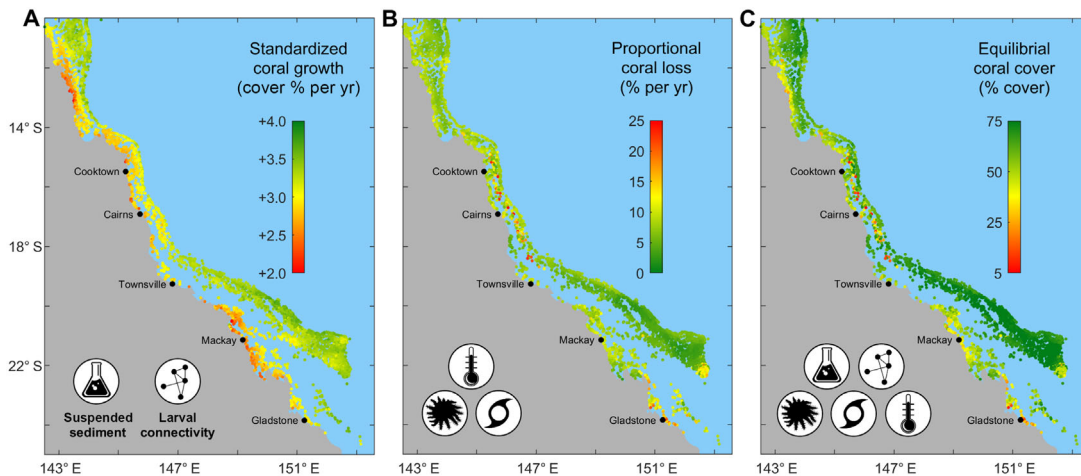


FIG. 10. (A) Annual growth rate of total coral cover based on GLM predictions from a standard 10% coral cover on all reefs with the reef-specific values of early life coral demographics (water-quality driven) and larval connectivity. (B) Long-term average mortality (mean annual proportional loss of total coral cover) due to CoTS, cyclones, and heat stress combined. (C) Equilibrational cover determined from long-term simulation of growth and average mortality.

individual impacts of acute stressors as proportional cover losses and quantified rates of coral recovery across the entire reefscape. Spatial patterns of standardized coral cover growth highlighted the influence of suspended sediments in creating cross-shelf disparities in the potential of coral recovery. The cumulative impacts of all stressors on simulated coral cover loss and recovery were captured within a single metric (equilibrium states) quantifying how much coral cover can be sustained on a reef given its forcing regime. Overall, our

study highlights the value of mechanistic simulations for cumulative impacts assessments and management on coral reefs.

GBR hindcast (2008–2020)

The reconstructed coral trajectories indicated a general decline of coral cover from ~29% to ~19%, equivalent to a loss of one-third of corals in 13 yr. The corresponding annual rate of absolute cover loss

simulated during 2008–2020 (-0.74% cover/yr) is greater than observed during 1985–2012 (-0.53% cover/yr) on 214 reefs (De'ath et al. 2012). Yet, the 1985–2012 assessment was based on manta-tow estimates of coral cover (De'ath et al. 2012) whereas our simulations are representative of transect-equivalent coral cover values, which are $\sim 7\%$ cover higher on average (Appendix S1). A more recent reconstruction produced a rate of annual cover loss of -1.92% cover/yr between 2009 and 2016 (Mellin et al. 2019) based on spatially explicit simulations of coral cover changes derived from transect-equivalent cover estimates. This rate of annual cover loss is considerably higher than the one estimated by our mechanistic simulations, yet it did not include the 2017 and 2020 bleaching events. However, inter-study comparisons are difficult as rates of absolute coral cover loss are dependent on pre-disturbance levels of coral cover, and different start and end points will capture a different sequence of disturbance events and recovery periods. Our reconstruction of coral trajectories also provides rates of coral loss that are independent of the fluctuating baseline cover, facilitating cross-study comparisons of the recent spatiotemporal coral dynamics on the GBR and providing a means to make future projections.

Our simulations also provide an assessment of coral reef health after the 2020 mass bleaching (Fig. 11A,

Appendix S2: Table S6). We found that 22% of reefs are in a critical state ($<10\%$ coral cover), 42% are in a poor state (10–20% coral cover), and only 19% are currently healthy ($>30\%$ coral cover). Recent manta-tow surveys across the mid- and outer-shelf Central GBR (AIMS 2020) indicate that, by June 2020, 42% of 33 monitored reefs were in a critical state, whereas only 12% would be considered healthy using the above benchmarks. Our predictions for the central region (excluding inshore reefs) yield a comparable figure based on 550 simulated reefs after conversion to manta-tow equivalent coral cover: 39% reefs in a critical state vs. 9% healthy.

Overall, the reconstructed trajectories exhibited a good agreement with the observed time-series of coral cover, recognizing that local discrepancies between reef-scale predictions and observations will inevitably arise. Some of these would constitute genuine errors in the model where a process is represented inappropriately, such as overlooking the contribution of key coral taxa to reefs' resistance and resilience, yet many will also reflect the substantive difficulty of capturing field forcing conditions in spatial layers. For example, while a cyclone track can be represented reasonably well, the dissipation of cyclone-induced wave energy around reef structures and islands is difficult to model accurately (Callaghan et al. 2020, Puotinen et al. 2020) and may fail to represent the conditions

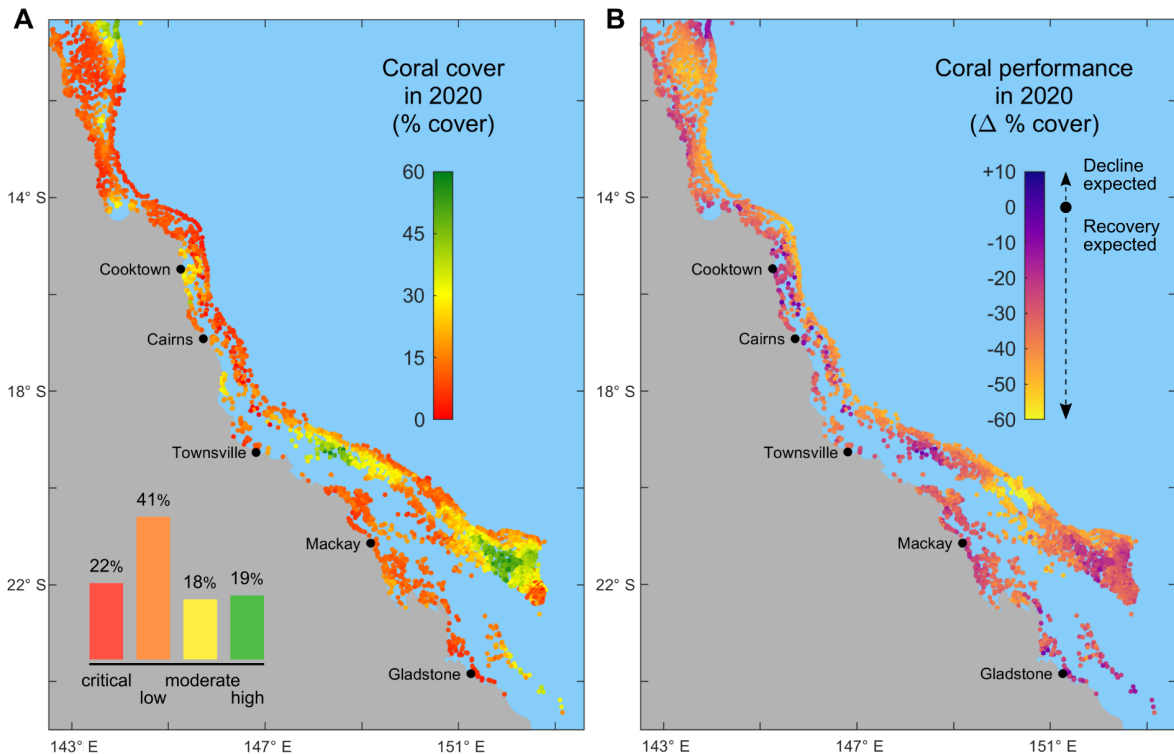


FIG. 11. (A) Present-day (2020) model predictions of total coral cover. Inset: GBR-wide distribution of reef health status: critical ($<10\%$ coral cover), low (10–20%), moderate (20–30%), high ($>30\%$). (B) Coral performance in 2020 as the difference between total coral cover and simulated equilibrium coral cover. A positive performance value indicates that present-day coral cover on a reef is greater than expected under its regime of disturbance and recovery; a decline is expected in a near future. Inversely, underperforming reefs (i.e., negative performance values) are expected to recover closer or beyond their equilibrium.

experienced by the reef from which coral cover measurements were taken. Moreover, storm damage is very patchy (Fabricius et al. 2008, Beeden et al. 2015), generating variable reef responses (Fig. 2C). Hence, the most frequent model errors were due to inaccuracies in the predicted occurrence (false positives and negatives) or intensity of storm damages rather than an inappropriate demographic parameterization.

Inaccurate spatial predictions can also arise from the necessary simplification of complex coral assemblages. With coral demographic rates being representative of species typically found on offshore reef habitats, the model may misrepresent coral cover on some inshore reefs (DeVantier et al. 2006, Browne et al. 2012). In addition, characteristics of larval dispersal were modeled based on acroporid life history, but other broadcast spawner species have different traits (gamete buoyancy, larval survivorship, and competency period) that would affect their exposure to SSC and dispersal potential. Incorporating turbidity-tolerant coral species, as well as a broader range of dispersal characteristics including aspects of the reproduction and dispersal of brooding species, would improve model realism on inshore reef habitats. Finally, efficient herbivore control of macroalgae was assumed despite evidence of abundant macroalgae on some inshore reefs (De'ath and Fabricius 2010, Thompson et al. 2019, Ceccarelli et al. 2020). How much this simplification affects coral cover predictions will depend on whether seaweed dominance on those reefs is persistent or transitory (Diaz-Pulido et al. 2009, Cheal et al. 2010). In future, with the integration of further processes affecting reefs locally (e.g., macroalgal production driven by nutrient concentration predicted by eReefs, habitat-specific levels of grazing), we expect the predictive capacity of ReefMod-GBR will improve.

Drivers of coral loss

Measured in terms of absolute coral loss, bleaching was the most important stressor GBR-wide during 2008–2020 (–2.5% cover/yr), accounting for 49% of the stress-induced coral loss, ahead of cyclones (–1.9% cover/yr, 40%) and CoTS outbreaks (–0.4% cover/yr, 11%). Manta-tow surveys (De'ath et al. 2012) for 1985–2012 found bleaching and CoTS accounted for, respectively, 10% and 42% of disturbance-driven coral mortality (see also Osborne et al. 2011 for similar figures using AIMS transect surveys between 1995 and 2009). The relative contribution of cyclones during 2008–2020 was similar to 1985–2012 (40% vs. 48%, respectively). The importance of cyclone impacts during both periods was partly driven by the considerable span of damage produced by TC Hamish (2009) in the Southern GBR, a severe cyclone with an unusual (coast-parallel) track. The sensitivity analysis performed on the reconstructed coral trajectories of monitored reefs revealed that cyclones had a greater influence than bleaching on the quality of model fits. Yet, inaccuracies in the prediction of cyclone

exposure generated important departures to the observed coral cover, and reefs affected by bleaching may have been under-represented in available monitoring data, especially in the northern region and after the 2020 marine heat wave. With three extreme heat waves over 2008–2020 vs. only two over 1985–2012, it is no surprise that bleaching accounted for a greater share of stress-induced coral mortality in our study. We note, however, that our simulation of mass bleaching relies on mortalities observed at ~2 m depth (Hughes et al. 2018), so represent the upper tail of the potential stress at ~5–10 m depths. Indeed, the incidence of bleaching can decrease substantially with depth due to the attenuation of light stress (Baird et al. 2018a).

In the last 5 yr, our simulations indicate that mass coral bleaching has caused successively a proportional loss of 44% (2016–2017 combined) and 40% (2020) of the pre-bleaching coral cover across the entire GBR. The fact that only 10% of the GBR escaped significant bleaching-induced mortality (<20% proportional loss) raises important concerns about the ability of the GBR to cope with more frequent and intense heat stress under a warming climate (e.g., Wolff et al. 2018). Our simulations indicated that the southern region had regained most of its pre-2009 (TC Hamish) coral cover by the onset of the 2020 mass bleaching, despite significant loss caused by TC Marcia in 2015. In the northern region, the marine heat wave in 2020 erased three years of recovery (+8.4% cover) that followed the successive impacts of the 2016–2017 bleaching events. With a 59% proportional reduction of coral cover from 2008 to 2020, northern reefs are the main losers of the past decade. Clearly, anthropogenic bleaching has now become a key driver of coral mortality across the GBR, threatening its ability to recover from other stressors.

Simulated impacts of CoTS outbreaks were relatively minor during 2008–2020 compared to previous assessments (–1.4% cover/yr; De'ath et al. 2012), although this period has coincided with the onset (in 2010) of the fourth cycle of CoTS outbreak since the 1960s (Pratchett et al. 2014). Given that CoTS density has been surveyed for only 2% of the GBR, we relied on the random initialization of CoTS populations derived from the spatial predictions of the CoCoNet model (Condie et al. 2018) with the subsequent dynamics driven by larval dispersal and coral abundance. The importance of nutrient-enhanced larval survival in the initiation of CoTS outbreaks is still debated (Pratchett et al. 2014, 2017, Wolfe et al. 2017), and it is noteworthy that the predicted survival of CoTS larvae during eight spawning seasons (2010–2018) was very low in the Cairns–Cooktown area (Fig. 3A, Appendix S3: Fig. S11), a region where all four CoTS outbreaks appear to have initiated (Brodie et al. 2005, Pratchett et al. 2014). Comparisons between eReefs predictions and in situ measurements have revealed a tendency of the model to locally underestimate nutrient and chlorophyll concentrations (Robson et al. 2020). On the other hand, CoTS likely started their

gradual build-up several years before the first detection of outbreaking densities in 2010. Unfortunately, available eReefs predictions do not capture the large river floods that occurred in this region during the 2008 and 2009 spawning seasons (Fabricius et al. 2010).

High chlorophyll concentrations were prevalent in the southern section of the GBR (Swains and Capricorn/Bunker sectors), both on inner and outer reefs (Appendix S3: Fig. S10). Inshore, this is likely due to runoff events with a culmination during the 2010–2011 wet season (Appendix S3: Fig. S11), and this has facilitated the propagation of CoTS populations created at initialization, although there is currently no evidence of CoTS outbreaks on southern inner reefs (Thompson et al. 2019). On southern offshore reefs, high chl *a* is likely the result of recurrent intrusions of nutrient-rich waters by upwelling on the shelf break (e.g., Andrews and Furnas 1986, Berkelmans et al. 2010), and it has been hypothesized that primary outbreaks could emerge there with no relation to river-flood events (Moran et al. 1988, Johnson 1992, Miller et al. 2015). Although the causes of primary outbreaks on the GBR are yet to be resolved (Pratchett et al. 2014, 2017), the present model can be used to explore the timing and mechanisms of the propagation of secondary outbreaks facilitated by nutrient availability (Brodie et al. 2017).

Drivers of coral recovery

The population growth rates that emerged from colony-scale simulations revealed which environmental factors contributed most to the expansion of coral cover. First and foremost is the influence of initial coral cover, which determines the subsequent rate of increase in coral cover, corroborating empirical observations (Graham et al. 2011, Ortiz et al. 2018). With a fixed rate of radial extension, the areal growth increment is greater for larger colonies than for smaller ones, so that, at least at the initial stage of coral colonization, the rate of cover growth becomes gradually faster as corals get bigger. As large and sexually mature colonies become more prevalent, self-recruitment intensifies because more offspring are produced, so that population size increases and amplifies the rate of cover growth. Subsequently, coral colonization reduces the space available for recruitment (Fig. 2B) and colony extension, thereby slowing down the rate of increase in coral cover until the colonization space is saturated (Fig. 9A). As a result, the influence of initial coral cover on subsequent growth is nonlinear and creates a sigmoid recovery curve (Fig. 2A) that is typically observed in *Acropora*-dominated communities (Halford et al. 2004, Emslie et al. 2008). We captured these dynamics at the community scale, first through the statistical modeling of the stepwise changes of total coral cover, then using the resulting model (GLM) to predict cover growth increments and reconstruct coral recovery curves. This enabled the integration of influential drivers of coral growth such as suspended sediments (Fig. 9B)

and allowed the systematic exploration of the potential of coral recovery across the entire reefscape (Fig. 10A). This growth model offers an alternative to heuristic inferences of recovery dynamics based on statistical model fits that depend on data availability (Thompson and Dolman 2010, Osborne et al. 2011, 2017, Wolff et al. 2018, Mellin et al. 2019).

Once standardized with the GLM, spatial variations in the simulated coral growth revealed the negative impacts of suspended sediments on the recovery potential of inshore reefs. This is consistent with recent empirical analyses (Ortiz et al. 2018, MacNeil et al. 2019) that found reductions in coral cover growth rates with the extent of river flood plumes assessed by satellite imagery. We note, however, that high SSC values can also result from wind-driven resuspension of fine sediments as observed during the dry season (Appendix S3: Fig S4B). Our assessment of water-quality impacts is based on predictions of transport, sinking, and resuspension of fine (30 μm) sediments from hydrodynamic modeling. This enables SSC exposure to be integrated over time periods (days to months) that are relevant to the sensitive stages of coral ontogeny (Humanes et al. 2017a, b), allowing physiological impacts to be scaled up to the ecosystem level. Retaining 10 yr as a standard recovery time under good water-quality conditions (mean annual SSC < 0.3 mg/L, corresponding to 10% of inshore reefs), our simulations indicate that an increment of 1 mg/L of steady-state SSC retards coral recovery by 9 months (Fig. 9B). While these predictions can help setting water-quality targets for management, they are likely biased toward a specific response of acroporids and remain to be tested in situ. However, detecting these impacts on coral cover is challenging; it would require extended time series as the deleterious effects of SSC might only become apparent after a long period of uninterrupted recovery. Hence, the sensitivity analysis revealed that integration of SSC impacts had a negligible influence on the quality of model fits to monitored coral trajectories, most likely because prediction errors are more sensitive to acute coral loss than differences in coral recovery rates. Although being representative of steady-state SSC exposures (annual averages at 4 km resolution), our simulated recovery rates are standardized to a given coral cover and can be used to compare the recovery potential (Fig. 10A) and resilience (Fig. 10C) among reefs.

Although larval connectivity is widely regarded as an important driver of coral recovery, a quantitative link between larval supply and coral cover dynamics is yet to be established. Here, variability in external larval supply had little influence on the reconstructed coral cover growth. With the current parameterization of larval retention (i.e., a minimum 28% of larvae produced by a reef is retained), the contribution of external supply to total settlement is globally low: based on the transition probabilities (i.e., without accounting for the actual number of larvae produced), external supply represented 6% of larval supply for 50% of all reefs (mean: 15% out of 3,806

reefs). Because coral settlement was modeled as a saturating function of larval supply, self-supply was generally sufficient for the making of settlement. This does not imply that external larval supply is not demographically important: after severe coral mortality, the relative influence of self-recruitment would likely decrease, making external supply a key process for local recovery. Moreover, considerable uncertainty exists in the set value of larval retention, with likely variations from reef to reef (Black 1993). We note, however, that the prediction of coral recovery matched observational data under the current model parameterization of which self-retention was the dominant component of coral recruitment. Furthermore, high self-retention of coral larvae is suggested by current experimental evidence (Sammarco and Andrews 1989). Future work should model larval dispersal at a finer spatial resolution (i.e., <1 km) for a better evaluation of the relative contribution of self vs. external supply. This information is critical to capture the demographic impacts of larval connectivity and support connectivity-based management interventions.

Other factors, not included in the model, have the potential to influence coral recovery. First, under insufficient herbivore grazing, macroalgae can bloom after widespread coral mortality and inhibit coral recovery (McManus and Polsenberg 2004, Mumby and Steneck 2008). Yet, on the GBR, herbivorous fish are a negligible catch (Smith et al. 2007, Bradford et al. 2019) and their importance in preventing coral-macroalgal phase shift is difficult to quantify (Cheal et al. 2010). Second, acute disturbances have lagged effects on surviving coral colonies that can hinder subsequent coral recovery. Prior bleaching stress can reduce coral fecundity (Ward et al. 2002) over multiple succeeding years (Levitan et al. 2014, Johnston et al. 2020). A similar effect on coral fecundity has been reported for multiple coral taxa after Cyclone Nathan in the Northern GBR (Baird et al. 2018b). However, because thermal stress mostly occurred toward the end of the hindcast, including the sublethal effects of acute stress would most likely have limited impact on the reconstructed trajectories. Similarly, the effects of ocean acidification were considered negligible over such a short period of time in comparison to the other stressors. Nevertheless, using the model for long-term simulations would require integrating all these effects on coral demographics for reliable projections of coral cover under climate change.

Cumulative impacts on coral loss and recovery

Expressing stress-induced coral mortality as proportional loss was key to assessing the spatial distribution of the individual and combined impacts of acute disturbances. This yielded vulnerability maps that reflect the frequency and intensity of recent disturbances contextualized within the coral community composition predicted by the model, while being independent of the levels of coral cover at the time of disturbances. The spatial

predictions of standardized coral growth and stress-induced coral mortality allowed computation of the equilibrium state for >3,800 reefs. Equilibrium states can be viewed as long-term averages around which coral cover fluctuates in a given reef environment. They integrate the combined effects of chronic (water quality) and acute stress (bleaching, cyclones, and CoTS), and their use here is to reveal spatial variability in the resilience of the ecosystem (Fig. 10C). Yet, since coral reefs are non-equilibrium systems that frequently experience acute impacts (Done 1992, Connell 1997), the transient state of reefs can be far higher or lower than their long-term equilibrium. With this in mind, the notion of equilibrium state differs from the concept of carrying capacity (the intrinsic limit of a population) as a reef can exhibit episodically higher levels of coral cover until stress-induced mortality brings the reef closer to its equilibrium cover value.

Although equilibria were created by running the model for 100 yr, they do not constitute projections for future reef health; they merely set regional expectations for the relative state of the system based on recent stress intensities and frequencies. Like for any resilience metric, transient stress regimes clearly challenge these expectations (i.e., intensifying heat stress), and projecting equilibrium states would require integrating specific forecast scenarios of disturbances into their calculation. Nevertheless, equilibria are useful for detecting shifting baselines through time: departures from the current estimates would indicate that reef resilience is eroding or, hopefully, improving. Because it integrates the stress and recovery environment that fluctuates over time, the equilibrium state is a more accurate indication of a reef's baseline than a snapshot survey of coral condition.

As an important note, the present metric of reef resilience does not account for competitive interactions (e.g., with macroalgae or soft corals) that will favor emergence of multiple equilibrium states (McManus and Polsenberg 2004, Mumby et al. 2007). Because coral dynamics under efficient grazing exhibit a single equilibrium state, equilibrium covers cannot reflect the vulnerability of reefs to coral-algal phase shifts, a growing concern in regions subject to overfishing. Earlier implementations of the model in the Caribbean (Mumby et al. 2007, 2014, Bozec and Mumby 2015, Bozec et al. 2016) show that reliable data on herbivore grazing allows calculation of a probability of coral-algal phase shifts for multiple environmental forcing and disturbance regimes. Future model versions will spatially integrate grazing and macroalgal productivity to assess this operational metric of ecological resilience (sensu Holling 1996: the ability to move toward alternate community types) and define ecological thresholds of coral persistence (Mumby et al. 2007, Bozec et al. 2016) across the GBR.

Mechanistic approach to cumulative effects assessment

Cumulative impacts on coral reefs have been traditionally assessed through the analysis of monitored coral

cover changes attributed to specific stressors. Yet, disentangling the individual effects of multiple drivers requires extensive monitoring data due to inherent difficulties in attributing causality to observed coral changes (Fabricius and De'ath 2004). Moreover, impacts that manifest as a slowing down of coral growth are easily overlooked by monitoring. While these can be evidenced at the scale of individual colonies in controlled environments, experimental designs can only manipulate a small number of stressors and have a limited ability to infer responses at the community level (Hodgson and Halpern 2019). Here, the core mechanisms underlying coral demography were simulated at the scale of coral colonies to quantify stressor impacts on specific biological processes and developmental life stages. This enabled the emergence of complex interactions and feedbacks that compound the cumulative effects of multiple drivers and determine the dynamics of coral cover. While incomplete knowledge on key demographic parameters has inhibited individual-based approaches for cumulative impacts assessments on coral reefs, we address this issue by providing a suite of empirical relationships between common stressors and coral demographics to promote a mechanistic evaluation of reef health. Moreover, the model can be applied to other regional settings, provided that the intensity of the integrated stressors (SSC, DHW, storm severity, CoTS density) is provisioned in time and space. Demographic parameters and responses to stressors can be refined with local empirical data or revisited according to the reef habitat represented (e.g., deeper reefs).

Cumulative impact assessments are often conducted by mapping overlapping stressors and combining them into cumulative threat or vulnerability indices (e.g., Halpern et al. 2015, Tulloch et al. 2015). While this generally assumes additivity of stressor effects, multiple stressors that affect different demographic processes can be difficult to combine and sometimes result in complex responses (e.g., antagonistic or synergistic). Here, we show that mechanistic simulations integrating key demographic processes and spatial information on stress exposure can address this complexity by evaluating the dynamics of biological responses across multiple spatial scales. They can be used to assess the relative importance of individual stressors and to provide insights on their interactions with other drivers. As a simulation tool, mechanistic models extend the scope of cumulative effects assessments by enabling the reconstruction of past population trends, projecting future changes for scenario analysis while allowing controlled manipulations of stressors on a scale infeasible in experiments.

Credible spatial mechanistic models have large data requirements in terms of spatial information but also for the parameterization of biological processes. Note that this does not imply perfect mechanistic knowledge overall; what holds is that given our current knowledge on how demographic mechanisms operate individually, we can aim to understand how they interact in driving biological populations virtually. Testing these predictions empirically

will be difficult at any scale, yet the grounding in underlying mechanisms combined with the successful validation of model behavior provides a basis for making future predictions outside of the input model parameter space. With the accelerating pace of environmental changes, this is critical for producing credible predictions under novel driver conditions (Gustafson et al. 2013).

Implications for reef monitoring and resilience-based management

Managing for coral resilience requires evaluating the current state of reefs, their exposure to disturbances and their ability to recover from those pressures. Our simulations predict the current state of >3,800 reefs on the GBR based on mechanistic expectations and spatiotemporal data on drivers. They provide an assessment in space and time of the stress regime of each reef covering both chronic environmental forcing (water quality and larval connectivity) and acute mortality events. This portfolio of reef vulnerability across the GBR can be combined with present-day spatial predictions of coral cover (Fig. 11A), community composition and demographic structure, and potential for coral recovery (incorporating exposure to CoTS and loose coral rubble) to complement reef monitoring. This is especially important considering that existing monitoring only represents ~40% only of the environmental regimes of the GBR (Mellin et al. 2020). While the present model informs about recent trends and status of unmonitored reef areas (~96% of the 3,806 reefs between 2008 and 2020), it can also help designing more representative and efficient coral and CoTS surveillance programs in support of reef management.

Of particular significance for an improved management of the GBR is the equilibrium cover as a metric of reef resilience. In principle, this measure provides a null model of geographic trends in reef state that represents the current stress and recovery environment. While recognizing the limits of predicting coral cover for non-equilibrium systems, equilibrium states set expectations of future changes in the short term: a coral cover value higher than the reef's equilibrium state indicates that the reef is performing better than expected, a performance that is unlikely to persist. Inversely, a reef that is largely under-performing relative to its equilibrium state is expected to recover higher than the equilibrium value. Comparing the current and potential performance of reefs (Fig. 11B) may help identify those most likely to respond to interventions and sustain improvements over the longer term. Note that a difference between observed and predicted coral states, as well as their respective distance to the expected equilibrium, may not only be due to inaccuracies in the predicted forcing or habitat type, but also to a local driver not included in the modeled dynamics. To this view, the model provides a means to detect reef "outliers" that deviate from the set expectations, which has the potential to promote model development but also to inform reef management (Cinner et al. 2016).

Finally, ReefMod-GBR offers a simulation tool to evaluate management scenarios and develop a structured decision-making process (Gregory et al. 2012). The model is already being used to explore spatial strategies and benefits of coral restoration, CoTS culling and control of anchor damage on the GBR under climate warming scenarios (Bozec and Mumby 2019, Mason et al. 2020, Fletcher et al. 2021). Benefits of management interventions can be measured in time and space using an array of model variables (e.g., coral cover, mortality and recovery rates, CoTS density). The equilibrium cover of a reef, as an operational metric capturing changes in cumulative impacts in response to a given intervention, offers new perspectives for evaluating the potential benefits of management scenarios and conduct spatial prioritization analyses. Equilibrium cover pertains to the associated regime of disturbance, so that a relaxation of acute (e.g., CoTS control) and chronic stress (e.g., water-quality improvement) would lead to a different equilibrium. Expanding the model with projections of carbon emissions will provide opportunities for exploring management strategies under climate change, and for prioritizing tactical interventions with the greatest benefits to the resilience of the GBR.

ACKNOWLEDGMENTS

This research was funded by the Australian Research Council (ARC) Centre of Excellence for Coral Reef Studies, the Great Barrier Reef Foundation (GBRF), an ARC Discovery Project, the Australian Government's National Environmental Science Programme (NESP 4.5 and 3.1.1), the Reef Restoration and Adaptation Project (RRAP) case, and a government consortium (Department of Environment, GBRMPA and the Queensland Government) to P. J. Mumby, Y.-M. Bozec, and K. Hock. The current field used for connectivity calculations and the sediment and chlorophyll fields were developed in the *eReefs* Project, a public-private collaboration between Australia's leading operational and scientific research agencies, government, and corporate Australia. We thank C. Doropoulos, G. Roff, N. Wolff, K. R. N. Anthony, and B. Schaffelke for fruitful discussions. Graphics of corals and CoTS courtesy of the Integration and Application Network, University of Maryland Center for Environmental Science.

LITERATURE CITED

- AIMS (Australian Institute of Marine Science). 2020. Annual Summary Report on coral reef condition for 2019/20. Long-term Reef Monitoring Program. Australian Institute of Marine Science, Townsville, Queensland, Australia.
- Andrews, J. C., and M. J. Furnas. 1986. Subsurface intrusions of Coral Sea water into the central Great Barrier Reef-I. Structures and shelf-scale dynamics. *Continental Shelf Research* 6:491–514.
- Babcock, R. C., G. D. Bull, P. L. Harrison, A. J. Heyward, J. K. Oliver, C. C. Wallace, and B. L. Willis. 1986. Synchronous spawnings of 105 scleractinian coral species on the Great Barrier Reef. *Marine Biology* 90:379–394.
- Babcock, R. C., and C. N. Mundy. 1992. Reproductive biology, spawning and field fertilization rates of *Acanthaster planci*. *Marine and Freshwater Research* 43:525–533.
- Baird, A. H., et al. 2018a. A decline in bleaching suggests that depth can provide a refuge from global warming in most coral taxa. *Marine Ecology Progress Series* 603:257–264.
- Baird, A. H., M. Álvarez-Noriega, V. R. Cumbo, S. R. Connolly, M. Dornelas, and J. S. Madin. 2018b. Effects of tropical storms on the demography of reef corals. *Marine Ecology Progress Series* 606:29–38.
- Baird, A. H., and P. Marshall. 2002. Mortality, growth and reproduction in scleractinian corals following bleaching on the Great Barrier Reef. *Marine Ecology Progress Series* 237:133–141.
- Baird, M. E., M. P. Adams, J. Andrewartha, N. Cherukuru, M. Gustafsson, S. Hadley, M. Herzfeld, E. Jones, N. Margvelashvili, and M. Mongin. 2017. CSIRO environmental modelling suite: scientific description of the optical, carbon chemistry and biogeochemical models (BGC1p0). <https://research.csiro.au/ereefs/wp-content/uploads/sites/34/2015/08/eReefsOpticalBGCframeBGC1p0.pdf>
- Ban, S. S., N. A. Graham, and S. R. Connolly. 2014. Evidence for multiple stressor interactions and effects on coral reefs. *Global Change Biology* 20:681–697.
- Baria, M. V. B., R. D. Villanueva, and J. R. Guest. 2012. Spawning of three-year-old *Acropora millepora* corals reared from larvae in northwestern Philippines. *Bulletin of Marine Science* 88:61–62.
- Beeden, R., J. Maynard, M. Puotinen, P. Marshall, J. Dryden, J. Goldberg, and G. Williams. 2015. Impacts and recovery from severe tropical Cyclone Yasi on the Great Barrier Reef. *PLoS One* 10:e0121272.
- Berkelmans, R. 2002. Time-integrated thermal bleaching thresholds of reefs and their variation on the Great Barrier Reef. *Marine Ecology Progress Series* 229:73–82.
- Berkelmans, R., G. De'ath, S. Kininmonth, and W. J. Skirving. 2004. A comparison of the 1998 and 2002 coral bleaching events on the Great Barrier Reef: spatial correlation, patterns, and predictions. *Coral Reefs* 23:74–83.
- Berkelmans, R., S. J. Weeks, and C. R. Steinberg. 2010. Upwelling linked to warm summers and bleaching on the Great Barrier Reef. *Limnology and Oceanography* 55:2634–2644.
- Biggs, B. C. 2013. Harnessing natural recovery processes to improve restoration outcomes: an experimental assessment of sponge-mediated coral reef restoration. *PLoS One* 8:e64945.
- Bindoff, N. L., et al. 2013. Detection and attribution of climate change: from global to regional. Pages 867–952 in T. F. Stocker, D. Qin, G.-K. Plattner, M. Tignor, S. Allen, J. Boschung, A. Nauels, Y. Xia, V. Bex, and P. M. Midgley, editors. *Climate change 2013: the physical science basis. Contribution of working group I to the fifth assessment report of the intergovernmental panel on climate change*. Cambridge University Press, Cambridge, UK.
- Birkeland, C., and J. Lucas. 1990. *Acanthaster planci*: major management problem of coral reefs. CRC Press, Boca Raton, Florida, USA.
- Black, K. P. 1993. The relative importance of local retention and inter-reef dispersal of neutrally buoyant material on coral reefs. *Coral Reefs* 12:43–53.
- Bozec, Y.-M., L. Alvarez-Filip, and P. J. Mumby. 2015. The dynamics of architectural complexity on coral reefs under climate change. *Global Change Biology* 21:223–235.
- Bozec, Y.-M., C. Doropoulos, G. Roff, and P. J. Mumby. 2019. Transient grazing and the dynamics of an unanticipated coral-algal phase shift. *Ecosystems* 22:296–311.
- Bozec, Y.-M., K. Hock, R. A. B. Mason, M. E. Baird, C. Castro-Sanguino, S. A. Condie, M. Puotinen, A. Thompson, and P. J. Mumby. 2021a. Code of the simulation model ReefMod-GBR (REEFMOD.6.4) (v.1.0.0). Zenodo. <http://dx.doi.org/10.5281/zenodo.5146037>
- Bozec, Y.-M., K. Hock, R. A. B. Mason, M. E. Baird, C. Castro-Sanguino, S. A. Condie, M. Puotinen, A. Thompson,

- and P.J. Mumby. 2021b. Data and code for ReefMod-GBR hindcast analyses (v1.0.0). Zenodo. <http://doi.org/10.5281/zenodo.5146061>
- Bozec, Y.-M., and P. J. Mumby. 2015. Synergistic impacts of global warming on the resilience of coral reefs. *Philosophical Transactions of the Royal Society B* 370:20130267.
- Bozec, Y.-M., and P. J. Mumby. 2019. Detailed description of ReefMod-GBR and simulation results. Pages 72–113 in Reef restoration and adaptation program: modelling methods and findings. A report provided to the Australian Government. Townsville, Queensland, Australia. https://www.gbrrestoration.org/documents/20182/20686/T6+Modelling+Methods+and+Findings_26April_FINAL3.pdf/88351cb3-aaa3-49ef-886b-b9f3fd474eba
- Bozec, Y. M., and P. J. Mumby. 2020. Coral reef models as assessment and reporting tools for the Reef 2050 Integrated Monitoring and Reporting Program—a review. Great Barrier Reef Marine Park Authority. <http://elibrary.gbrmpa.gov.au/jspui/bitstream/11017/3570/7/Coral%20Reef%20Supplementary%20Report%207.pdf>
- Bozec, Y.-M., S. O'Farrell, J. H. Bruggemann, B. E. Luckhurst, and P. J. Mumby. 2016. Tradeoffs between fisheries harvest and the resilience of coral reefs. *Proceedings of the National Academy of Sciences USA* 113:4536–4541.
- Bradford, T., K. Wolfe, and P. J. Mumby. 2019. Preferences and perceptions of the recreational spearfishery of the Great Barrier Reef. *PLoS One* 14:e0221855.
- Brodie, J., M. Devlin, and S. Lewis. 2017. Potential enhanced survivorship of crown of thorns starfish larvae due to near-annual nutrient enrichment during secondary outbreaks on the central mid-shelf of the Great Barrier Reef, Australia. *Diversity* 9:17.
- Brodie, J., K. Fabricius, G. De'ath, and K. Okaji. 2005. Are increased nutrient inputs responsible for more outbreaks of crown-of-thorns starfish? An appraisal of the evidence. *Marine Pollution Bulletin* 51:266–278.
- Brodie, J., and J. Waterhouse. 2012. A critical review of environmental management of the 'not so Great' Barrier Reef. *Estuarine, Coastal and Shelf Science* 104:1–22.
- Browne, N. K., S. G. Smithers, and C. T. Perry. 2012. Coral reefs of the turbid inner-shelf of the Great Barrier Reef, Australia: an environmental and geomorphic perspective on their occurrence, composition and growth. *Earth-Science Reviews* 115:1–20.
- Callaghan, D. P., P. J. Mumby, and M. S. Mason. 2020. Near-reef and nearshore tropical cyclone wave climate in the Great Barrier Reef with and without reef structure. *Coastal Engineering* 157:103652.
- Ceccarelli, D. M., R. D. Evans, M. Logan, P. Mantel, M. Puotinen, C. Petus, G. R. Russ, and D. H. Williamson. 2020. Long-term dynamics and drivers of coral and macroalgal cover on inshore reefs of the Great Barrier Reef Marine Park. *Ecological Applications* 30:e02008.
- Cheal, A. J., M. A. MacNeil, E. Cripps, M. J. Emslie, M. Jonker, B. Schaffelke, and H. Sweatman. 2010. Coral-macroalgal phase shifts or reef resilience: links with diversity and functional roles of herbivorous fishes on the Great Barrier Reef. *Coral Reefs* 29:1005–1015.
- Cheal, A. J., M. A. MacNeil, M. J. Emslie, and H. Sweatman. 2017. The threat to coral reefs from more intense cyclones under climate change. *Global Change Biology* 23:1511–1524.
- Cinner, J. E., et al. 2016. Bright spots among the world's coral reefs. *Nature* 535:416–419.
- Condie, S. A., É. E. Plagányi, E. B. Morello, K. Hock, and R. Beeden. 2018. Great Barrier Reef recovery through multiple interventions. *Conservation Biology* 32:1356–1367.
- Connell, J. H. 1997. Disturbance and recovery of coral assemblages. *Coral Reefs* 16:S101–S113.
- Connolly, S. R., and A. H. Baird. 2010. Estimating dispersal potential for marine larvae: dynamic models applied to scleractinian corals. *Ecology* 91:3572–3583.
- Côté, I. M., J. A. Gill, T. A. Gardner, and A. R. Watkinson. 2005. Measuring coral reef decline through meta-analyses. *Philosophical Transactions of the Royal Society B* 360:385–395.
- Crain, C. M., K. Kroeker, and B. S. Halpern. 2008. Interactive and cumulative effects of multiple human stressors in marine systems. *Ecology Letters* 11:1304–1315.
- Darling, E. S., and I. M. Côté. 2008. Quantifying the evidence for ecological synergies. *Ecology Letters* 11:1278–1286.
- Darling, E. S., T. R. McClanahan, and I. M. Côté. 2013. Life histories predict coral community disassembly under multiple stressors. *Global Change Biology* 19:1930–1940.
- De'ath, G., and K. Fabricius. 2010. Water quality as a regional driver of coral biodiversity and macroalgae on the Great Barrier Reef. *Ecological Applications* 20:840–850.
- De'ath, G., K. E. Fabricius, H. Sweatman, and M. Puotinen. 2012. The 27-year decline of coral cover on the Great Barrier Reef and its causes. *Proceedings of the National Academy of Sciences USA* 109:17995–17999.
- De'ath, G., and P. J. Moran. 1998. Factors affecting the behaviour of crown-of-thorns starfish (*Acanthaster planci* L.) on the Great Barrier Reef: 2: Feeding preferences. *Journal of Experimental Marine Biology and Ecology* 220:107–126.
- DeVantier, L. M., G. De'ath, E. Turak, T. J. Done, and K. E. Fabricius. 2006. Species richness and community structure of reef-building corals on the nearshore Great Barrier Reef. *Coral Reefs* 25:329–340.
- Diaz-Pulido, G., L. J. McCook, S. Dove, R. Berkelmans, G. Roff, D. I. Kline, S. Weeks, R. D. Evans, D. H. Williamson, and O. Hoegh-Guldberg. 2009. Doom and boom on a resilient reef: climate change, algal overgrowth and coral recovery. *PLoS One* 4:e5239.
- Done, T. J. 1992. Phase shifts in coral reef communities and their ecological significance. *Hydrobiologia* 247:121–132.
- Done, T. J. 1995. Ecological criteria for evaluating coral reefs and their implications for managers and researchers. *Coral Reefs* 14:183–192.
- Doropoulos, C., G. Roff, Y.-M. Bozec, M. Zupan, J. Werninghausen, and P. J. Mumby. 2016. Characterizing the ecological trade-offs throughout the early ontogeny of coral recruitment. *Ecological Monographs* 86:20–44.
- Doropoulos, C., S. Ward, G. Roff, M. González-Rivero, and P. J. Mumby. 2015. Linking demographic processes of juvenile corals to benthic recovery trajectories in two common reef habitats. *PLoS One* 10:e0128535.
- Eakin, C. M., J. A. Morgan, S. F. Heron, T. B. Smith, G. Liu, L. Alvarez-Filip, B. Baca, E. Bartels, C. Bastidas, and C. Bouchon. 2010. Caribbean corals in crisis: record thermal stress, bleaching, and mortality in 2005. *PLoS One* 5:e13969.
- Edmunds, P. J., and B. Riegl. 2020. Urgent need for coral demography in a world where corals are disappearing. *Marine Ecology Progress Series* 635:233–242.
- Edwards, H. J., I. A. Elliott, C. M. Eakin, A. Irikawa, J. S. Madin, M. McField, J. A. Morgan, R. van Woesik, and P. J. Mumby. 2011. How much time can herbivore protection buy for coral reefs under realistic regimes of hurricanes and coral bleaching? *Global Change Biology* 17:2033–2048.
- Emslie, M., A. Cheal, H. Sweatman, and S. Delean. 2008. Recovery from disturbance of coral and reef fish communities on the Great Barrier Reef, Australia. *Marine Ecology Progress Series* 371:177–190.
- Engelhardt, U., M. Hartcher, J. Cruise, D. Engelhardt, M. Russell, N. Taylor, G. Thomas, and D. Wiseman. 1999. Finescale

- surveys of crown-of-thorns starfish (*Acanthaster planci*) in the central Great Barrier Reef region. Technical Report no. 30. CRC Reef Research Centre, Townsville, Queensland, Australia.
- Engelhardt, U., M. Hartcher, N. Taylor, J. Cruise, D. Engelhardt, M. Russel, I. Stevens, G. Thomas, D. Williamson, and D. Wiseman. 2001. Crown-of-thorns starfish (*Acanthaster planci*) in the central Great Barrier Reef region. Results of fine-scale surveys conducted in 1999–2000. Technical Report no. 32. CRC Reef Research Centre, Townsville, Queensland, Australia.
- Evans, R. D., et al. 2020. Early recovery dynamics of turbid coral reefs after recurring bleaching events. *Journal of Environmental Management* 268:110666.
- Fabricius, K. E. 2005. Effects of terrestrial runoff on the ecology of corals and coral reefs: review and synthesis. *Marine Pollution Bulletin* 50:125–146.
- Fabricius, K. E., and G. De'ath. 2004. Identifying ecological change and its causes: a case study on coral reefs. *Ecological Applications* 14:1448–1465.
- Fabricius, K. E., G. De'ath, M. L. Puotinen, T. Done, T. F. Cooper, and S. C. Burgess. 2008. Disturbance gradients on inshore and offshore coral reefs caused by a severe tropical cyclone. *Limnology and Oceanography* 53:690–704.
- Fabricius, K., K. Okaji, and G. De'ath. 2010. Three lines of evidence to link outbreaks of the crown-of-thorns seastar *Acanthaster planci* to the release of larval food limitation. *Coral Reefs* 29:593–605.
- Filbee-Dexter, K., and T. Wernberg. 2018. Rise of turfs: a new battleground for globally declining kelp forests. *BioScience* 68:64–76.
- Fletcher, C. S., C. Castro-Sanguino, S. Condie, Y.-M. Bozec, K. Hock, D. W. Gladish, P. J. Mumby, and D. A. Westcott. 2021. Regional-scale modelling capability for assessing crown-of-thorns starfish control strategies on the Great Barrier Reef. Reef and Rainforest Research Centre Limited, Cairns, Queensland, Australia. <https://nesptropical.edu.au/wp-content/uploads/2021/03/NESP-TWQ-Project-5.1-Technical-Report-3.pdf>
- Fox, H. E., J. S. Pet, R. Dahuri, and R. L. Caldwell. 2003. Recovery in rubble fields: long-term impacts of blast fishing. *Marine Pollution Bulletin* 46:1024–1031.
- Fox, R. J., and D. R. Bellwood. 2007. Quantifying herbivory across a coral reef depth gradient. *Marine Ecology Progress Series* 339:49–59.
- GBRMPA (Great Barrier Reef Marine Park Authority). Great Barrier Reef Outlook Report 2019. GBRMPA, Townsville, Queensland, Australia.
- GBRMPA (Great Barrier Reef Marine Park Authority). 2007. Great Barrier Reef (GBR) Features (Reef boundaries, QLD Mainland, Islands, Cays, Rocks and Dry Reefs). eAtlas. <https://eatlas.org.au/data/uuid/ac8e8e4f-fc0e-4a01-9c3d-f27e4a8fac3c>
- Graham, N. A., S. Jennings, M. A. MacNeil, D. Mouillot, and S. K. Wilson. 2015. Predicting climate-driven regime shifts versus rebound potential in coral reefs. *Nature* 518:94–97.
- Graham, N. A. J., K. L. Nash, and J. T. Kool. 2011. Coral reef recovery dynamics in a changing world. *Coral Reefs* 30:283–294.
- Gregory, R., L. Failing, M. Harstone, G. Long, T. McDaniels, and D. Ohlson. 2012. Structured decision making: a practical guide to environmental management choices. Wiley-Blackwell, Oxford, UK.
- Gunderson, L. H., and C. S. Holling. 2002. Panarchy: understanding transformations in human and natural systems. Island Press, Washington, D.C., USA.
- Gustafson, E. J. 2013. When relationships estimated in the past cannot be used to predict the future: using mechanistic models to predict landscape ecological dynamics in a changing world. *Landscape Ecology* 28:1429–1437.
- Haddon, M. 2011. Modelling and quantitative methods in fisheries. CRC Press/Chapman and Hall, Boca Raton, Florida, USA.
- Halford, A., A. J. Cheal, D. Ryan, and D. M. B. Williams. 2004. Resilience to large-scale disturbance in coral and fish assemblages on the great barrier reef. *Ecology* 85:1892–1905.
- Hall, V., and T. Hughes. 1996. Reproductive strategies of modular organisms: comparative studies of reef-building corals. *Ecology* 77:950–963.
- Halpern, B. S., et al. 2015. Spatial and temporal changes in cumulative human impacts on the world's ocean. *Nature Communications* 6:1–7.
- Halpern, B. S., and R. Fujita. 2013. Assumptions, challenges, and future directions in cumulative impact analysis. *Ecosphere* 4:1–11.
- Harborne, A. R., A. Rogers, Y. M. Bozec, and P. J. Mumby. 2017. Multiple stressors and the functioning of coral reefs. *Annual Review of Marine Science* 9:445–468.
- Heron, S., et al. 2016. Validation of reef-scale thermal stress satellite products for coral bleaching monitoring. *Remote Sensing* 8:59.
- Herzfeld, M., et al. 2016. eReefs marine modelling: final report. CSIRO, Hobart, Tasmania, Australia.
- Hock, K., C. Doropoulos, R. Gorton, S. A. Condie, and P. J. Mumby. 2019. Split spawning increases robustness of coral larval supply and inter-reef connectivity. *Nature Communications* 10:3463.
- Hock, K., N. H. Wolff, J. C. Ortiz, S. A. Condie, K. R. Anthony, P. G. Blackwell, and P. J. Mumby. 2017. Connectivity and systemic resilience of the Great Barrier Reef. *PLoS Biology* 15:e2003355.
- Hodgson, E. E., and B. S. Halpern. 2019. Investigating cumulative effects across ecological scales. *Conservation Biology* 33:22–32.
- Hoegh-Guldberg, O., et al. 2007. Coral reefs under rapid climate change and ocean acidification. *Science* 318:1737–1742.
- Holling, C. S. 1996. Engineering resilience versus ecological resilience. Pages 31–43 in P. Schulze, editor. *Engineering within ecological constraints*. National Academic Press, Washington, D.C., USA.
- Hughes, T. P. 2011. Shifting base-lines, declining coral cover, and the erosion of reef resilience: comment on Sweatman et al. (2011). *Coral Reefs* 30:653–660.
- Hughes, T. P., et al. 2003. Climate change, human impacts, and the resilience of coral reefs. *Science* 301:929–933.
- Hughes, T. P., et al. 2017. Global warming and recurrent mass bleaching of corals. *Nature* 543:373.
- Hughes, T. P., et al. 2018. Global warming transforms coral reef assemblages. *Nature* 556:492.
- Hughes, T. P., and J. H. Connell. 1999. Multiple stressors on coral reefs: A long-term perspective. *Limnology and Oceanography* 44:932–940.
- Hughes, T. P., and J. E. Tanner. 2000. Recruitment failure, life histories, and long-term decline of Caribbean corals. *Ecology* 81:2250–2263.
- Humanes, A., A. Fink, B. L. Willis, K. E. Fabricius, D. de Beer, and A. P. Negri. 2017a. Effects of suspended sediments and nutrient enrichment on juvenile corals. *Marine Pollution Bulletin* 125:166–175.
- Humanes, A., G. F. Ricardo, B. L. Willis, K. E. Fabricius, and A. P. Negri. 2017b. Cumulative effects of suspended sediments, organic nutrients and temperature stress on early life

- history stages of the coral *Acropora tenuis*. *Scientific Reports* 7:44101.
- Johnson, C. 1992. Settlement and recruitment of *Acanthaster planci* on the Great Barrier Reef: questions of process and scale. *Marine and Freshwater Research* 43:611–627.
- Johnston, E. C., C. W. Counsell, T. L. Sale, S. C. Burgess, and R. J. Toonen. 2020. The legacy of stress: coral bleaching impacts reproduction years later. *Functional Ecology* 34:2315–2325.
- Jones, R., G. Ricardo, and A. Negri. 2015. Effects of sediments on the reproductive cycle of corals. *Marine Pollution Bulletin* 100:13–33.
- Keesing, J. K., and A. R. Halford. 1992. Importance of postsettlement processes for the population dynamics of *Acanthaster planci* (L.). *Marine and Freshwater Research* 43:635–651.
- Keesing, J., and J. Lucas. 1992. Field measurement of feeding and movement rates of the crown-of-thorns starfish *Acanthaster planci* (L.). *Journal of Experimental Marine Biology and Ecology* 156:89–104.
- Kettle, B., and J. Lucas. 1987. Biometric relationships between organ indices, fecundity, oxygen consumption and body size in *Acanthaster planci* (L.) (Echinodermata; Asteroidea). *Bulletin of Marine Science* 41:541–551.
- Kuffner, I. B., L. J. Walters, M. A. Becerro, V. J. Paul, R. Ritson-Williams, and K. S. Beach. 2006. Inhibition of coral recruitment by macroalgae and cyanobacteria. *Marine Ecology Progress Series* 323:107–117.
- Lam, V. Y., M. Chaloupka, A. Thompson, C. Doropoulos, and P. J. Mumby. 2018. Acute drivers influence recent inshore Great Barrier Reef dynamics. *Proceedings of the Royal Society B* 285:20182063.
- Levitán, D. R., W. Boudreau, J. Jara, and N. Knowlton. 2014. Long-term reduced spawning in *Orbicella* coral species due to temperature stress. *Marine Ecology Progress Series* 515:1–10.
- Liu, G., W. J. Skirving, E. F. Geiger, J. L. De La Cour, B. L. Marsh, S. F. Heron, K. V. Tirak, A. E. Strong, and C. M. Eakin. 2017. NOAA Coral Reef Watch's 5km satellite coral bleaching heat stress monitoring product suite version 3 and four-month outlook version 4. *Reef Encounter* 32:39–45.
- Loya, Y., K. Sakai, K. Yamazato, Y. Nakano, H. Sambali, and R. Van Woesik. 2001. Coral bleaching: the winners and the losers. *Ecology Letters* 4:122–131.
- Lucas, J. S. 1984. Growth, maturation and effects of diet in *Acanthaster planci* (L.) (Asteroidea) and hybrids reared in the laboratory. *Journal of Experimental Marine Biology and Ecology* 79:129–147.
- MacNeil, M. A., C. Mellin, S. Matthews, N. H. Wolff, T. R. McClanahan, M. Devlin, C. Drovandi, K. Mengersen, and N. A. Graham. 2019. Water quality mediates resilience on the Great Barrier Reef. *Nature Ecology & Evolution* 3:620–627.
- MacNeil, M. A., C. Mellin, M. S. Pratchett, J. Hoey, K. R. Anthony, A. J. Cheal, I. Miller, H. Sweatman, Z. L. Cowan, and S. Taylor. 2016. Joint estimation of crown of thorns (*Acanthaster planci*) densities on the Great Barrier Reef. *PeerJ* 4:e2310.
- Madin, J. S., A. H. Baird, M. Dornelas, and S. R. Connolly. 2014. Mechanical vulnerability explains size-dependent mortality of reef corals. *Ecology Letters* 17:1008–1015.
- Margvelashvili, N., et al. 2018. Simulated fate of catchment-derived sediment on the Great Barrier Reef shelf. *Marine Pollution Bulletin* 135:954–962.
- Mason, R., K. de la Motte, Y.-M. Bozec, M. Adams, and P. J. Mumby. 2020. Resilience-based management tools for the Great Barrier Reef. Reef and Rainforest Research Centre Limited, Cairns, Queensland, Australia. https://eprints.qut.edu.au/208585/1/Mason_et_al_2020_NESP_Report.pdf
- McManus, J. W., and J. F. Polsenberg. 2004. Coral–algal phase shifts on coral reefs: ecological and environmental aspects. *Progress in Oceanography* 60:263–279.
- Mellin, C., et al. 2019. Spatial resilience of the Great Barrier Reef under cumulative disturbance impacts. *Global Change Biology* 25:2431–2445.
- Mellin, C., E. Peterson, M. Puotinen, and B. Schaffelke. 2020. Representation and complementarity of the long-term coral monitoring on the Great Barrier Reef. *Ecological Applications* 30:e02122.
- Miller, I., H. Sweatman, A. Cheal, M. Emslie, K. Johns, M. Jonker, and K. Osborne. 2015. Origins and implications of a primary crown-of-thorns starfish outbreak in the southern Great Barrier Reef. *Journal of Marine Biology* 2015:1–10.
- Moran, P. J. 1986. The *Acanthaster* phenomenon. *Oceanography and Marine Biology: an Annual Review* 24:379–480.
- Moran, P. J., R. H. Bradbury, and R. E. Reichelt. 1988. Distribution of recent outbreaks of the crown-of-thorns starfish (*Acanthaster planci*) along the Great Barrier Reef: 1985–1986. *Coral Reefs* 7:125–137.
- Moran, P., and G. De'ath. 1992. Estimates of the abundance of the crown-of-thorns starfish *Acanthaster planci* in outbreaking and non-outbreaking populations on reefs within the Great Barrier Reef. *Marine Biology* 113:509–515.
- Mumby, P. J. 1999. Bleaching and hurricane disturbances to populations of coral recruits in Belize. *Marine Ecology Progress Series* 190:27–35.
- Mumby, P. J. 2006. The impact of exploiting grazers (Scaridae) on the dynamics of Caribbean coral reefs. *Ecological Applications* 16:747–769.
- Mumby, P. J., A. Hastings, and H. J. Edwards. 2007. Thresholds and the resilience of Caribbean coral reefs. *Nature* 450:98–101.
- Mumby, P. J., and R. S. Steneck. 2008. Coral reef management and conservation in light of rapidly evolving ecological paradigms. *Trends in Ecology & Evolution* 23:555–563.
- Mumby, P. J., N. H. Wolff, Y.-M. Bozec, I. Chollett, and P. Hal-loran. 2014. Operationalizing the resilience of coral reefs in an era of climate change. *Conservation Letters* 7:176–187.
- Okaji, K. 1996. Feeding ecology in the early life stages of the crown-of-thorns starfish, *Acanthaster planci* (L.). Thesis, James Cook University, Townsville, Queensland, Australia.
- Ortiz, J. C., Y.-M. Bozec, N. H. Wolff, C. Doropoulos, and P. J. Mumby. 2014. Global disparity in the ecological benefits of reducing carbon emissions for coral reefs. *Nature Climate Change* 4:1090.
- Ortiz, J.-C., N. H. Wolff, K. R. Anthony, M. Devlin, S. Lewis, and P. J. Mumby. 2018. Impaired recovery of the Great Barrier Reef under cumulative stress. *Science Advances* 4:eaar6127
- Osborne, K., A. M. Dolman, S. C. Burgess, and K. A. Johns. 2011. Disturbance and the dynamics of coral cover on the Great Barrier Reef (1995–2009). *PLoS One* 6:e17516.
- Osborne, K., A. A. Thompson, A. J. Cheal, M. J. Emslie, K. A. Johns, M. J. Jonker, M. Logan, I. R. Miller, and H. Sweatman. 2017. Delayed coral recovery in a warming ocean. *Global Change Biology* 23:3869–3881.
- Paine, R. T., M. J. Tegner, and E. A. Johnson. 1998. Compounded perturbations yield ecological surprises. *Ecosystems* 1:535–545.
- Pratchett, M. S. 1999. An infectious disease in crown-of-thorns starfish on the Great Barrier Reef. *Coral Reefs* 18:272.
- Pratchett, M. S. 2005. Dynamics of an outbreak population of *Acanthaster planci* at Lizard Island, northern Great Barrier Reef (1995–1999). *Coral Reefs* 24:453–462.
- Pratchett, M. S. 2010. Changes in coral assemblages during an outbreak of *Acanthaster planci* at Lizard Island, northern Great Barrier Reef (1995–1999). *Coral Reefs* 29:717–725.

- Pratchett, M., et al. 2017. Thirty years of research on Crown-of-Thorns Starfish (1986–2016): scientific advances and emerging opportunities. *Diversity* 9:41.
- Pratchett, M. S., C. F. Caballes, J. A. Rivera-Posada, and H. P. Sweatman. 2014. Limits to understanding and managing outbreaks of crown-of-thorns starfish (*Acanthaster* spp.). *Oceanography and Marine Biology: An Annual Review* 52:133–200.
- Puotinen, M., E. Drost, R. Lowe, M. Depczynski, B. Radford, A. Heyward, and J. Gilmour. 2020. Towards modelling the future risk of cyclone wave damage to the world's coral reefs. *Global Change Biology* 26:4302–4315.
- Puotinen, M., J. A. Maynard, R. Beeden, B. Radford, and G. J. Williams. 2016. A robust operational model for predicting where tropical cyclone waves damage coral reefs. *Scientific Reports* 6:26009.
- Rasser, M., and B. Riegl. 2002. Holocene coral reef rubble and its binding agents. *Coral Reefs* 21:57–72.
- Richmond, R. H. 1997. Reproduction and recruitment in corals: critical links in the persistence of reefs. Pages 175–197 in C. E. Birkeland, editor. *Life and death of coral reefs*. Chapman & Hall, New York, New York, USA.
- Robson, B., J. Skerratt, M. Baird, C. Davies, M. Herzfeld, E. Jones, M. Mongin, A. Richardson, F. Rizwi, and K. Wild-Allen. 2020. Enhanced assessment of the eReefs biogeochemical model for the Great Barrier Reef using the Concept/State/Process/System model evaluation framework. *Environmental Modelling & Software* 129:104707.
- Sammarco, P. W., and J. C. Andrews. 1989. The Helix experiment: differential localized dispersal and recruitment patterns in Great Barrier Reef corals. *Limnology and Oceanography* 34:896–912.
- Sano, M., M. Shimizu, and Y. Nose. 1987. Long-term effects of destruction of hermatypic corals by *Acanthaster planci* infestation on reef fish communities at Iriomote Island, Japan. *Marine Ecology Progress Series* 37:191–199.
- Schaffelke, B., J. Carleton, M. Skuza, I. Zagorskis, and M. J. Furnas. 2012. Water quality in the inshore Great Barrier Reef lagoon: Implications for long-term monitoring and management. *Marine Pollution Bulletin* 65:249–260.
- Schaffelke, B., C. Collier, F. Kroon, J. Lough, L. McKenzie, M. Ronan, S. Uthicke, and J. Brodie. 2017. Chapter 1: The condition of coastal and marine ecosystems of the Great Barrier Reef and their responses to water quality and disturbances. *Scientific consensus statement 2017. A synthesis of the science of land-based water quality impacts on the Great Barrier Reef*. State of Queensland, Brisbane, Queensland, Australia. https://www.reefplan.qld.gov.au/_data/assets/pdf_file/0030/45993/2017-scientific-consensus-statementsummary-chap01.pdf
- Smith, T., C. McCormack, J. Kung, and M. Dunning. 2007. Ecological risk assessment of the other species component of the coral reef fin fish fishery. Queensland Department of Primary Industries and Fisheries, Brisbane, Queensland, Australia.
- Sweatman, H. H., A. A. Cheal, G. G. Coleman, M. M. Emslie, K. K. Johns, M. M. Jonker, I. I. Miller, and K. K. Osborne. 2008. Long-term monitoring of the great barrier reef, status report 8. Australian Institute of Marine Science, Townsville, Queensland, Australia.
- Sweatman, H., S. Delean, and C. Syms. 2011. Assessing loss of coral cover on Australia's Great Barrier Reef over two decades, with implications for longer-term trends. *Coral Reefs* 30:521–531.
- Thompson, A., P. Costello, J. Davidson, M. Logan, and G. Coleman. 2019. Marine Monitoring Program: Annual report for inshore coral reef monitoring 2017–18. Australian Institute of Marine Science: Report for the Great Barrier Reef Marine Park Authority. Great Barrier Reef Marine Park Authority, Townsville, Queensland, Australia.
- Thompson, A. A., and A. M. Dolman. 2010. Coral bleaching: one disturbance too many for near-shore reefs of the Great Barrier Reef. *Coral Reefs* 29:637–648.
- Thompson, A., T. Schroeder, V. E. Brando, and B. Schaffelke. 2014. Coral community responses to declining water quality: Whitsunday Islands, Great Barrier Reef, Australia. *Coral Reefs* 33:923–938.
- Trapon, M. L., M. S. Pratchett, and A. S. Hoey. 2013. Spatial variation in abundance, size and orientation of juvenile corals related to the biomass of parrotfishes on the Great Barrier Reef, Australia. *PLoS One* 8:e57788.
- Tulloch, V. J. D., et al. 2015. Why do we map threats? Linking threat mapping with actions to make better conservation decisions. *Frontiers in Ecology and the Environment* 13:91–99.
- Vercelloni, J., K. Mengersen, F. Ruggeri, and M. J. Caley. 2017. Improved coral population estimation reveals trends at multiple scales on Australia's Great Barrier Reef. *Ecosystems* 20:1337–1350.
- Viehman, T. S., J. L. Hench, S. P. Griffin, A. Malhotra, K. Egan, and P. N. Halpin. 2018. Understanding differential patterns in coral reef recovery: chronic hydrodynamic disturbance as a limiting mechanism for coral colonization. *Marine Ecology Progress Series* 605:135–150.
- Walker, B., L. Gunderson, A. Kinzig, C. Folke, S. Carpenter, and L. Schultz. 2006. A handful of heuristics and some propositions for understanding resilience in social-ecological systems. *Ecology and Society* 11:13.
- Ward, S., P. Harrison, and O. Hoegh-Guldberg. 2002. Coral bleaching reduces reproduction of scleractinian corals and increases susceptibility to future stress. Pages 1123–1128 in *Proceedings of the Ninth International Coral Reef Symposium*, Bali, 23–27 October 2000.
- Waterhouse, J., J. Brodie, D. Tracey, R. Smith, M. VanderGragt, C. Collier, C. Petus, M. Baird, F. Kroon, and R. Mann. 2017. Chapter 3: the risk from anthropogenic pollutants to Great Barrier Reef coastal and marine ecosystems. 2017 Scientific Consensus Statement: land use impacts on the Great Barrier Reef water quality and ecosystem condition. State of Queensland, Brisbane, Queensland, Australia. https://www.reefplan.qld.gov.au/_data/assets/pdf_file/0032/45995/2017-scientific-consensus-statementsummary-chap03.pdf
- White, J. W., A. Rassweiler, J. F. Samhouri, A. C. Stier, and C. White. 2014. Ecologists should not use statistical significance tests to interpret simulation model results. *Oikos* 123:385–388.
- Wolfe, K., A. Graba-Landry, S. A. Dworjanyan, and M. Byrne. 2017. Superstars: Assessing nutrient thresholds for enhanced larval success of *Acanthaster planci*, a review of the evidence. *Marine Pollution Bulletin* 116:307–314.
- Wolff, N. H., P. J. Mumby, M. Devlin, and K. Anthony. 2018. Vulnerability of the Great Barrier Reef to climate change and local pressures. *Global Change Biology* 24:1978–1991.
- Zann, L., J. Brodie, C. Berryman, and M. Naqasima. 1987. Recruitment, ecology, growth and behavior of juvenile *Acanthaster planci* (L.) (Echinodermata: Asteroidea). *Bulletin of Marine Science* 41:561–575.
- Zann, L., J. Brodie, and V. Vuki. 1990. History and dynamics of the crown-of-thorns starfish *Acanthaster planci* (L.) in the Suva area, Fiji. *Coral Reefs* 9:135–144.

SUPPORTING INFORMATION

Additional supporting information may be found online at: <http://onlinelibrary.wiley.com/doi/10.1002/ecm.1494/full>

OPEN RESEARCH

Computer code for model simulations (Bozec et al. 2021*a*) is available on Zenodo at <https://doi.org/10.5281/zenodo.5146037>. Code for analyses and data (Bozec et al. 2021*b*) are available on Zenodo at <https://doi.org/10.5281/zenodo.5146061>